University of California,
Irvine

The Search for Muon Neutrinos from Northern Hemisphere Gamma-Ray Bursts with AMANDA-II

Dissertation

submitted in partial satisfaction of the requirements
for the degree of

Doctor of Philosophy

in Physics and Astronomy

by

Kyler Kuehn

Dissertation Committee:
Professor Steven Barwick, Chair
Professor Henry Sobel
Professor Gaurang Yodh

2007

The dissertation of Kyler Kuehn
is approved and is acceptable in quality
and form for publication on microfilm:

Committee Chair

University of California, Irvine
2007

"And the sky begins to thunder
And I'm filled with awe and wonder
'Til the only burning question that remains
Is who am I?

Can I form a single mountain
Take the stars in hand and count them
Can I even take a breath
Without God giving it to me?"
—Steven Curtis Chapman

Table of Contents

List of Figures

List of Tables

My heartfelt gratitude goes out to Rebecca, my running buddy, my study buddy, my sailing skipper, my friend, my partner, my center, my present and my future, without whom my life would be immeasurably poorer.

To Lisa, without whom I never would have made it through grad school.

To Steve, without whom I would have had no direction over the last 7 years, and to the rest of the Barwick group for their daily support.

To Alex and Caroline, without whom I would not be sane.

To Francine, without whom the dissertation writing process would have been infinitely more burdensome.

To my family, especially Roger, Kay, Kevin, and Kerry, without whom I would not be who I am.

To those who have been a part of my spiritual family over the last seven years: Kirk Winslow, Mark Roberts, Michelle Jurlin, Adrien Lowery, Sharlynne Perry, Mary & Don Watson, Chris & Carolyn Anderson, Julie Aird, Brian Pitts, Heather Guenther, Elaine Storm, Beth Alamo, Sarah Gallon, Jenifer Carter Johnson, Tammy Bosler, and so many others without whom I would I would just be a resounding gong or a clashing cymbal, making much noise of no real significance.

To the instructors and advisors who have made a difference in my life, especially Vitaly Kresin, Steve Trullinger, Jack Feinberg, Matt Wood, Terry Oswalt, Lutz Köpke, Gary Hill, Amy Flatten, Thomas Habinek, Cochece Davis, Eddie Roth, and Ken Taylor.

I am also thankful to Eli Waxman and Kohta Murase for productive and thought-provoking input to this analysis, as well as Shantanu Desai for detailed discussions regarding the Super-Kamiokande GRB analysis.
The IceCube Collaboration acknowledges the support from the following agencies: National Science Foundation-Office of Polar Program, National Science Foundation-Physics Division, University of Wisconsin Alumni Research Foundation, Department of Energy, and National Energy Research Scientific Computing Center (supported by the Office of Energy Research of the Department of Energy), the NSF-supported TeraGrid system at the San Diego Supercomputer Center (SDSC), and the National Center for Supercomputing Applications (NCSA); Swedish Research Council, Swedish Polar Research Secretariat, and Knut and Alice Wallenberg Foundation, Sweden; German Ministry for Education and Research, Deutsche Forschungsgemeinschaft (DFG), Germany; Fund for Scientific Research (FNRS-FWO), Flanders Institute to encourage scientific and technological research in industry (IWT), Belgian Federal Office for Scientific, Technical and Cultural affairs (OSTC); the Netherlands Organisation for Scientific Research (NWO); M. Ribordy acknowledges the support of the SNF (Switzerland); J. D. Zornoza acknowledges the Marie Curie OIF Program (contract 007921).

KYLER KUEHN

1210 Palo Verde Rd kkuehn@uci.edu
Irvine, CA 92617 (949) 854-2267
http://www.ps.uci.edu/~kuehn

EDUCATION

Ph. D. Candidate in Physics (Experimental Astrophysics), University of California at Irvine
Expected Date of Completion: June 2007
M. S. Physics, University of California at Irvine, March 2002
B. A. Classical Civilization, University of Southern California, December 1999
B. S. Physics, University of Southern California, December 1998

PROFESSIONAL EXPERIENCE

Graduate Research Assistant
Department of Physics and Astronomy, University of California at Irvine
March 2000-Present
Duties include design and implementation of data analysis techniques for the Antarctic Muon and Neutrino Detector Array (AMANDA), with particular focus on the search for neutrinos from Gamma-Ray Bursts. Specific tasks involve development of experimental background rejection methods, software coding and implementation, and written and oral presentation of experimental results to scientific and non-scientific audiences. This position also involves independent and collaborative efforts with up to 200 other researchers and professors to facilitate AMANDA's continued successful operation.

Graduate Teaching Assistant
Department of Physics and Astronomy, University of California at Irvine
September 1999-Present (Intermittent Appointments)
Duties include classroom presentation and laboratory oversight for beginning and intermediate undergraduate students, along with examination preparation and grading. This position requires work with a team of 1-4 other teaching assistants and a professor to ensure effective presentation of material to classes of 20-300 students. (Profile of teaching experience available upon request.)

Assistant in Public Outreach
Department of Physics and Astronomy, University of California at Irvine
September 1999-Present
Duties include coordinating public viewing nights at the UCI Observatory for 200-5,000 visitors, facilitating individual observation periods for guests, and presenting "highlights of the night sky to large non-technical audiences. This position also involves overseeing private observatory tours for smaller groups (e.g. Girl Scout Troops) and providing multi-media presentations at off-site facilities (e.g. elementary schools), as well as delivering occasional professional

development seminars for high school science teachers interested in astronomy. In addition to organizational and public-speaking skills, requires considerable technical knowledge of both fixed and portable telescopes and general knowledge of "backyard astronomy".

Chair, International Organizing Committee
Second Canadian-American Mexican (CAM) Physics Graduate Student Conference
May 2004-May 2006
Duties include organizational oversight of conference agenda, scientific presentations, conference venue, grant applications, travel and hotel booking, and numerous other related details for the conference held in August, 2005. Significant collaborative skills were required to coordinate the efforts of the sixteen other members of the International and Local Organizing Committees. The scientific and social aspects of the conference were extremely well received by more than 100 graduate students and 15 plenary speakers attending from throughout North America.

Senior Learning Skills Assistant
California State Summer School for Math and Science, University of California at Irvine
June 2000-July 2002 (Summer Appointment)
The Summer School was a month-long full-time residential experience for advanced high school students gifted in science and mathematics. Duties included instruction of high school students in observational and data analysis skills via direct data collection with UCI's 0.8m telescope, as well as CLEA laboratory exercises. Required collaborative teaching with several other instructors, mastery of hardware and software for robotic telescope operation, and foundational knowledge in astrophysics and Windows/LINUX based data acquisition and analysis programs.

Research Assistant
Hydrodynamics Institute, Siberian Branch of the Russian Academy of Sciences
December 1998-February 1999
Duties included computational simulation of galactic structure formation and correlation with spiral galaxy observations. In addition, I assisted in translation and editing of works submitted by members of the Russian Academy of Sciences to English-speaking scholarly journals.

Undergraduate Research Assistant
Department of Physics and Astronomy, University of Southern California
January 1996-December 1998
Duties included design, integration, and operation of experimental apparatus components for time-of-flight mass spectroscopy measurements. Additional duties included assisting my research group in ongoing experiments and in

preparation of results for publication.

Undergraduate Research Assistant
Department of Physics and Astronomy, Florida Institute of Technology
Summer 1998
Duties included augmentation of existing computational codes for binary star interaction simulations, and correlation of results with Hubble Space Telescope and other observational data. This summer program culminated in a mini-conference where all participants presented research results and attended seminars focused on scientific ethics and professional expectations within the scientific community.

Undergraduate Research Assistant
Atomic, Molecular, and Optical Physics Summer School, Los Alamos National Laboratory
Summer 1997
Duties included analysis of observations from the Array of Low Energy X-Ray Imaging Sensors (ALEXIS) satellite, archival data searches, and correlation of ALEXIS results with several other ground- and space-based observatories. This summer program included daily lectures taught by visiting scientists in the forefront of research in atomic, molecular, and optical physics.

TECHNICAL SKILLS AND PROFESSIONAL ACTIVITIES

8+ years of research experience: experimental apparatus development, construction, maintenance, and software interfacing, in both independent and collaborative capacities.
Computer programming experience: C, Fortran, PAW, ROOT, IDL, LaTex, HTML, and PERL, with emphasis on astrophysical simulations and experimental data analysis techniques.
Proficiency in Windows and LINUX/UNIX environments.
15+ academic quarters of teaching assistant experience, at both the high school and college level, for both science and non-science majors. Significant experience in organization of professional scientific conferences.

Member, American Physical Society (APS), 1998-Present
Executive Board Member, APS Forum on Graduate Student Affairs, 2005-Present
Member, American Astronomical Society, 2002-Present
Member, American Scientific Affiliation, 2002-Present
Member, Astronomical Society of the Pacific, 2003-Present
Member, International Dark-Sky Association, 2004-Present

PUBLICATIONS AND PRESENTATIONS

PEER-REVIEWED ARTICLES:

The IceCube Collaboration (corresponding author **K. Kuehn**), "The Search for Muon Neutrinos from Northern Hemisphere Gamma-Ray Bursts with AMANDA", submitted to Ap. J. (astro-ph/0705.1186)

The IceCube Collaboration (including **K. Kuehn**), "Multi-Year Search for a Diffuse Flux of Muon Neutrinos with AMANDA-II", submitted to PRD (astro-ph/0705.1315)

The IceCube Collaboration (including **K. Kuehn**), "The Search for Neutrino Induced Cascades from Gamma Ray Bursts with AMANDA", Ap. J., in press (astro-ph/0702265)

The IceCube Collaboration (including **K. Kuehn**), "Five Years of Searches for Point Sources of Astrophysical Neutrinos with the AMANDA-II Neutrino Telescope", PRD, in press (astro-ph/0611063)

The IceCube Collaboration (including **K. Kuehn**), "On the Selection of AGN Neutrino Source Candidates for Source Stacking Analysis", Astropart. Phys., in press (astro-ph/0609534)

The IceCube Collaboration (including **K. Kuehn**) "Limits on the High Energy Gamma and Neutrino Fluxes from the SGR1806-20 Giant Flare of December 27^{th}, 2004 with the AMANDA-II Detector" (astro-ph/0607233)

The IceCube Collaboration (including **K. Kuehn**), "First Year Performance of the IceCube Neutrino Telescope", Astropart. Phys. Vol 26 (2006) 155-173, October 2006 (astro-ph/0604450)

The IceCube Collaboration (including **K. Kuehn**), "Optical Properties of Deep Glacial Ice at the South Pole", J. Geophys. Res. 111 (2006) D13203

The AMANDA Collaboration (including **K. Kuehn**), "Limits to Muon Flux from Neutralino Annihilations in the Sun", Astropart. Phys. Vol. 24 (2006) 459-466 (astro-ph/0508518)

The AMANDA Collaboration (including **K. Kuehn**), "The Search for Extraterrestrial Point Sources of High Energy Neutrinos with AMANDA-II Using Data Collected in 2000-2002", PRD 72 (2005) 077102 (astro-ph/0412347)

The AMANDA Collaboration (including **K. Kuehn**), "Flux Limits on Ultra High Energy Neutrinos with AMANDA-B10", Astropart. Phys. Vol. 22 (2004) 339-353

The AMANDA Collaboration (including **K. Kuehn**), "Search for neutrino-induced cascades with AMANDA", Astropart. Phys. Vol. 22 (2004) 127-138 (astro-ph/0405218)

The AMANDA Collaboration (including **K. Kuehn**), "Measurement of the cosmic ray composition at the knee with the SPASE-2/AMANDA-B10 detectors", Astropart. Phys. Vol. 21 (2004) 565-581

The AMANDA Collaboration (including **K. Kuehn**), "Search for Extraterrestrial Point Sources of Neutrinos with AMANDA-II", PRL 92 071102 (2004) (astro-ph/0309585)

The AMANDA Collaboration (including **K. Kuehn**), "Calibration and Survey of AMANDA with the SPASE Detectors", NIM A522 (2004) 347

The AMANDA Collaboration (including **K. Kuehn**), "Muon Track Reconstruction

and Data Selection Techniques in AMANDA", NIM A524 (2004) 169-194 (astro-ph/0407044)
The AMANDA Collaboration (including **K. Kuehn**), "Limits on Diffuse Fluxes of High Energy Extraterrestrial Neutrinos with the AMANDA B-10 Detector", PRL 90 (2003) 251101 (astro-ph/0303218)
The AMANDA Collaboration (including **K. Kuehn**), "Search for Point Sources of High Energy Neutrinos with AMANDA", Ap. J. 583 (2003) 1040-1057 (astro-ph/0208006)
The AMANDA Collaboration (including **K. Kuehn**), "Results from AMANDA", Mod. Phys. Lett. A17 (2002) 2019

CONFERENCE PRESENTATIONS:
K. Kuehn, "Multi-Messenger Astronomy with GLAST and IceCube", presented at the GLAST Users Workshop, Los Angeles, CA, May 2007
K. Kuehn for the IceCube Collaboration, "The Search for Neutrinos from GRBs with AMANDA", presented at the American Physical Society Meeting, Jacksonville, FL, April 2007.
K. Kuehn for the IceCube Collaboration, "The Search for Neutrinos from GRBs with AMANDA", presented at the October Astrophysics Conference "GRBs in the Swift Era", Washington D.C., December 2005. Also presented at the American Astronomical Society Meeting, Washington, D.C., January 2006.
K. Kuehn for the IceCube Collaboration, "The Search for Neutrinos from GRBs with AMANDA", presented at the Second Canadian-American-Mexican Graduate Physics Student Conference, San Diego, CA, August 2005.
K. Kuehn for the AMANDA Collaboration, "The Search for Neutrinos from Gamma-Ray Bursts with AMANDA", presented at the American Astronomical Society Meeting, San Diego, CA, January 2005.
K. Kuehn for the AMANDA Collaboration, "Recent Results in the Search for Neutrinos from Gamma-Ray Bursts", presented at the American Physical Society Division of Particles and Fields Meeting, Riverside, CA, August 2004.
K. Kuehn for the AMANDA Collaboration, "The Search for Neutrinos from Gamma-Ray Bursts with AMANDA", presented at the American Physical Society Meeting, Denver, CO, May 2004.
K. Kuehn for the AMANDA Collaboration, "The Search for Neutrinos from Gamma-Ray Bursts with AMANDA-B10 and AMANDA-II", presented at the Topics in Astroparticle and Underground Physics Conference, Seattle, WA, October 2003. Also presented at the Canada-America-Mexico International Graduate Student Conference, Merida, Mexico, October 2003.
K. Kuehn and A.M. Trubachev, "Detonation Waves: An Engine for Sequential Star Formation?", presented at the 3rd International Guillermo Haro Conference, Puebla, Mexico, November 1999.
K. Kuehn and M. Wood, "Taking the Pulse of SU UMa Stars", presented at the Southeastern Association for Research in Astronomy Meeting, Athens, Georgia, August 1998. Also published in the International Amateur and Professional Photoelectric Photometry Journal, Spring 1999.

K. Kuehn, "Multiwavelength Correlation of ALEXIS Observations, with Implications for Teaching and Research", presented at the American Association of Physics Teachers Annual Conference, New Orleans, LA, January 1998.

Abstract of the Dissertation

The Search for Muon Neutrinos from Northern Hemisphere Gamma-Ray Bursts
with AMANDA-II

By

Kyler Kuehn

Doctor of Philosophy in Physics and Astronomy

University of California, Irvine, 2007

Professor Steven Barwick, Chair

Abstract

We present the results of the analysis of neutrino observations by the Antarctic Muon and Neutrino Detector Array (AMANDA) correlated with photon observations of more than 400 gamma-ray bursts (GRBs) in the Northern Hemisphere from 1997 to 2003. During this time period, AMANDA's effective collection area for muon neutrinos was larger than that of any other existing detector. Based on our observations of zero neutrinos during and immediately prior to the GRBs in the dataset, we set the most stringent upper limit on muon neutrino emission correlated with gamma-ray bursts. Assuming a Waxman-Bahcall spectrum and incorporating all systematic uncertainties, our flux upper limit has a normalization at 1 PeV of

$E^2\Phi_\nu \leq 6.0 \times 10^{-9}$ GeVcm^{-2}s^{-1}sr^{-1},

with 90% of the events expected within the energy range of ~10 TeV to ~3 PeV. The impact of this limit on several theoretical models of GRBs is discussed, as well as the future potential for detection of GRBs by next generation neutrino telescopes. Finally, we briefly describe several modifications to this analysis in order to apply it to other types of transient point sources.

Chapter 1

Introduction

1.1 Gamma-Ray Bursts

Gamma-ray bursts (GRBs) are among the most energetic, and enigmatic, phenomena in the universe. The first GRB was detected by the Vela satellites (see Figure 1.1) in 1967, though we are only now beginning to unravel the mysteries of their origin. Based on their luminosity and the cosmological distances derived from redshift measurements of burst afterglows and/or host galaxies (Costa et al. , 2003), GRBs require the release of an enormous amount of energy (E $\approx 10^{53} \times \Omega/4\pi$ erg) (Frail et al. , 2001) in as little as a fraction of a second. Based on the observations of the Burst and Transient Source Experiment (BATSE) and other space-based detectors, they are expected to occur throughout the observable universe at a rate of $\gtrsim$700 per year, though current instruments do not have sufficient sky coverage or sensitivity to detect every burst. During its decade of operation, BATSE observed more than 2700 GRBs (Figure 1.2). Long duration ($\gtrsim$2 sec) bursts are believed to originate from the collapse of a massive stellar progenitor into a black hole, whereas short duration ($\lesssim$2 sec) bursts are believed to result from the merger of two compact objects into a black hole (Eicher et al. , 1989)[1]. Figure 1.3 depicts these two paths. Though these two types of bursts come from different progenitors, both are consistent with the canonical picture of gamma-ray bursts—the fireball scenario (Fryer & Mészáros , 2003; Piran , 2004). A fireball is generated during the formation of the black hole when the outflowing

[1]For a more recent treatment of the compact object merger scenario, see Paczyński (1998); Lewin et al. (2006), and for an alternative description of the GRB progenitor scenario, see also Roming et al. (2006).

plasma is accelerated to ultrarelativistic speeds. Subsequently, in an optically thin region (outside of the progenitor), the kinetic energy of the plasma is converted to radiation, either through interaction with an external medium or through self-interaction within the flow (Piran , 2002). If the circumstellar environment contains enough baryonic material, it will be entrained with the accelerated plasma[2]. Subsequent photo-pion production by baryon interaction with synchrotron or inverse Compton scattered photons will lead to several decay products, including muon neutrinos and antineutrinos in a ratio of 2:1. The primary reaction is:

$$p + \gamma \rightarrow \Delta \rightarrow \pi^{+} + n \tag{1.1}$$

followed by

$$\pi^{+} \rightarrow \mu^{+} + \nu_{\mu} \tag{1.2}$$

after which the muon will further decay to

$$\mu^{+} \rightarrow e^{+} + \nu_{e} + \bar{\nu_{\mu}}. \tag{1.3}$$

Similarly, "precursor" neutrinos may be generated by p–γ and p–nucleon interactions within the star and in the immediate circumburst environment (Razzaque et al. , 2003b). While the GRB jet is still within the stellar material, radiative losses of the accelerated material are low. The maximum energy for accelerated protons is, however, limited by synchrotron emission in the jet magnetic field to a few $\times 10^{9}$ GeV (or even lower, depending on the stellar progenitor). Similarly, electrons will be accelerated in the magnetic field, and their

[2]Alternate mechanisms for GRB emission, such as the "Poynting Flux–driven" bursts (Lyutikov & Blandford , 2003), are based upon electromagnetic rather than hydrodynamic sources of energy to power the burst. Such mechanisms do not predict significant acceleration of baryons in GRBs; thus, the expected neutrino flux from Poynting flux–driven bursts is essentially zero. A positive detection of GRB neutrinos is one clear way to differentiate these two mechanisms. We do not treat the E&M mechanism further in this work.

synchrotron photons will serve as the targets of interaction for the accelerated protons, while the "cold" protons not accelerated by the shocks are the targets for p-p interactions. Both interactions will lead to neutrino production through secondary pion decay, as described above.

Due to their minuscule interaction cross section (Gandhi et al. , 1998), neutrinos generated in gamma-ray bursts will reach the AMANDA detector after traveling nearly unimpeded from the burst environment. These neutrinos serve as a new messenger of astrophysical processes, providing information that is unattainable with conventional photon astronomy, or even other with other particle detectors (Figure 1.4). AMANDA has been searching for high-energy neutrinos from various astrophysical fluxes (both discrete and diffuse) for nearly a decade; in this work we focus on the analysis of AMANDA data correlated with photon observations of more than 400 GRBs from 1997 to 2003.

1.2 The AMANDA Detector

The AMANDA detector (Ahrens et al. , 2002) is an array of Optical Modules (OMs) deployed at depths between 1.5 and 2 km beneath the surface of the ice at the South Pole. An OM consists of a photomultiplier tube housed in a glass pressure sphere. During the years 1997-1999 the detector operated with 302 OMs on ten strings placed in a circular geometry with a diameter of about 100 m, and was known as AMANDA B-10. From 2000 onward, nine additional strings were in operation, placed within a diameter of about 200 m, bringing the total number of optical modules to 677 (see Figure 1.5). This phase of the neutrino observatory (dubbed AMANDA-II) operated through 2004, and continues as a high density component of IceCube, a km-scale detector currently being constructed (Achterberg et al. , 2006a).

The optical modules in AMANDA are designed to detect the Cherenkov emission from neutrino-induced muons that travel through or near the instrumented volume of ice (see Figure 1.6). While other neutrinos may be detected with this search, the efficiency for ν_e or ν_τ detection is significantly smaller. Other multi-flavor GRB neutrino searches which don't require directional information have been performed (Achterberg et al. , 2007); we focus here on the search for GRB muon neutrinos from the Northern Hemisphere. Due to the limited volume of ice above the detector, few downgoing extraterrestrial neutrinos will interact above and be detected by AMANDA. At the energies of interest to this analysis, the down-going events in the AMANDA dataset are primarily the atmospheric muon background which will completely overwhelm any potential downgoing signal. Thus, our extraterrestrial signal is primarily confined to the horizontal or up-going direction (Figure 1.7). As these muon neutrinos travel through the ice, they may interact with nearby nucleons to create energetic muons:

$$\nu_\mu + N \to \mu + X, \tag{1.4}$$

where N is a nucleon and X represents other reaction products. Muons produced in these interactions may carry a significant fraction of the original neutrino energy. Depending on its energy, the muon can travel up to tens of kilometers through the ice; for ν_μ in the energy range of greatest interest to AMANDA ($\sim 10^5$ GeV), the muon path length is $\sim$10 km (Lipari & Stanev , 1991).

Since AMANDA can detect such a muon anywhere along its substantial path length, the effective detector volume is significantly larger than the actual instrumented volume. A muon that has sufficient energy will continuously emit Cherenkov radiation, and will also generate additional particles due to stochastic processes. The ice at a depth of more than one kilometer is extremely clear, and thus the Cherenkov photons have large scattering (L_s^{eff}) and absorption (L_a) lengths—at λ = 400 nm, $L_s^{eff}\approx$25 m and $L_a\approx$100 m (Ackermann et al. , 2006). The Cherenkov light therefore has the potential to reach numerous OMs as the muon travels through the detector, and the relative timing of the hit OMs provides the basis for a set of maximum-likelihood reconstruction algorithms to determine the muon's direction of origin (Ahrens et al. , 2004). The algorithms applied to this analysis are based on variations from a randomly-seeded "first guess" track using the Pandel function to parametrize the sequence of OM hits. The likelihood of the initial track is calculated, and then the procedure is iterated (up to 32 times) to determine the most likely muon track. Iterations beyond the first incorporate increasingly complex features of the detector response to the Cherenkov photons, the details of which are beyond the scope of this work[3]. Detector simulations, along with observations of downgoing cosmic ray muons, have shown that this procedure provides track reconstructions accurate to within a mean value of ~2°. Atmospheric muons are almost entirely removed from the dataset by constraining our search to those bursts occurring in the Northern Hemisphere, allowing the detector to be shielded from a substantial background flux by the bulk of the earth. Upgoing atmospheric neutrinos caused by cosmic ray interactions in the northern hemisphere may also be detected by AMANDA, as their spectrum extends into the energy range of relevance to the GRB search. However, they likewise are removed from the dataset by requiring strict spatial and temporal correlation with photon observations of GRBs. With these selection criteria applied, we expect less than 0.01 atmospheric neutrino events in our dataset (Hodges , 2007).

In Chapter 2 we describe several models for GRB neutrino emission. In Chapter 3 we discuss the method for determining periods of stable detector performance and for separating the expected GRB neutrino signal from all misreconstructed

[3] An alternative track reconstruction known as a "paraboloid fit" is also relevant for our secondary data selection criteria, see Section 3.3 for further details.

background events, as well as the systematic uncertainties associated with this analysis procedure. In Chapter 4 we compare the results of the AMANDA observations with the models, as well as provide a spectrum-independent method for determining the fluence upper limit from GRBs. We conclude in Chapter 5 with the future potential of AMANDA/IceCube, for both the standard GRB search in the Swift era (Markwardt et al. , 2005) and for searches optimized for other transient point sources, such as jet-driven supernovae.

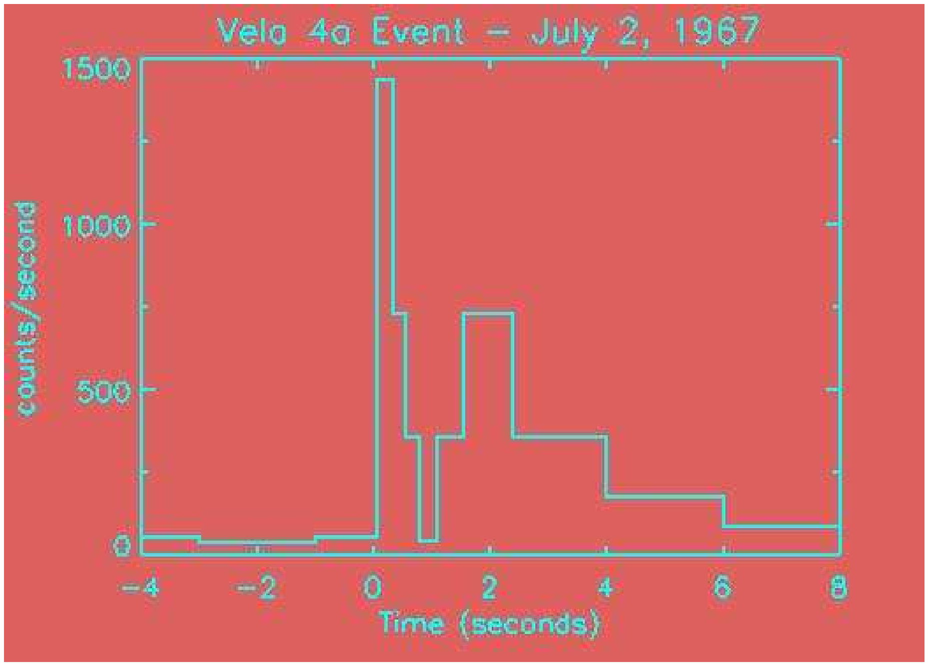

Figure 1.1: The first GRB, detected by the Vela satellites during their monitoring and verification of the nuclear test ban treaty.

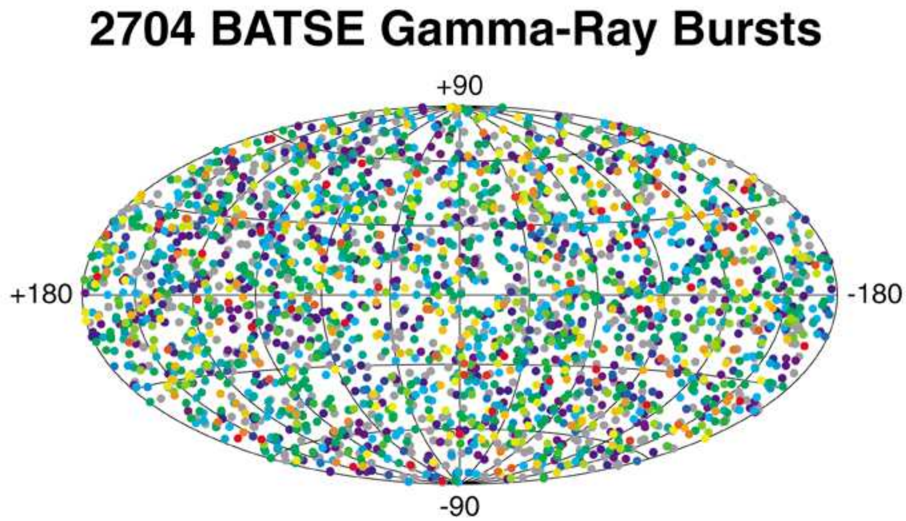

Figure 1.2: The 2704 GRBs of the BATSE 4B catalog, in galactic coordinates. Their uniform distribution attests to their cosmological origin.

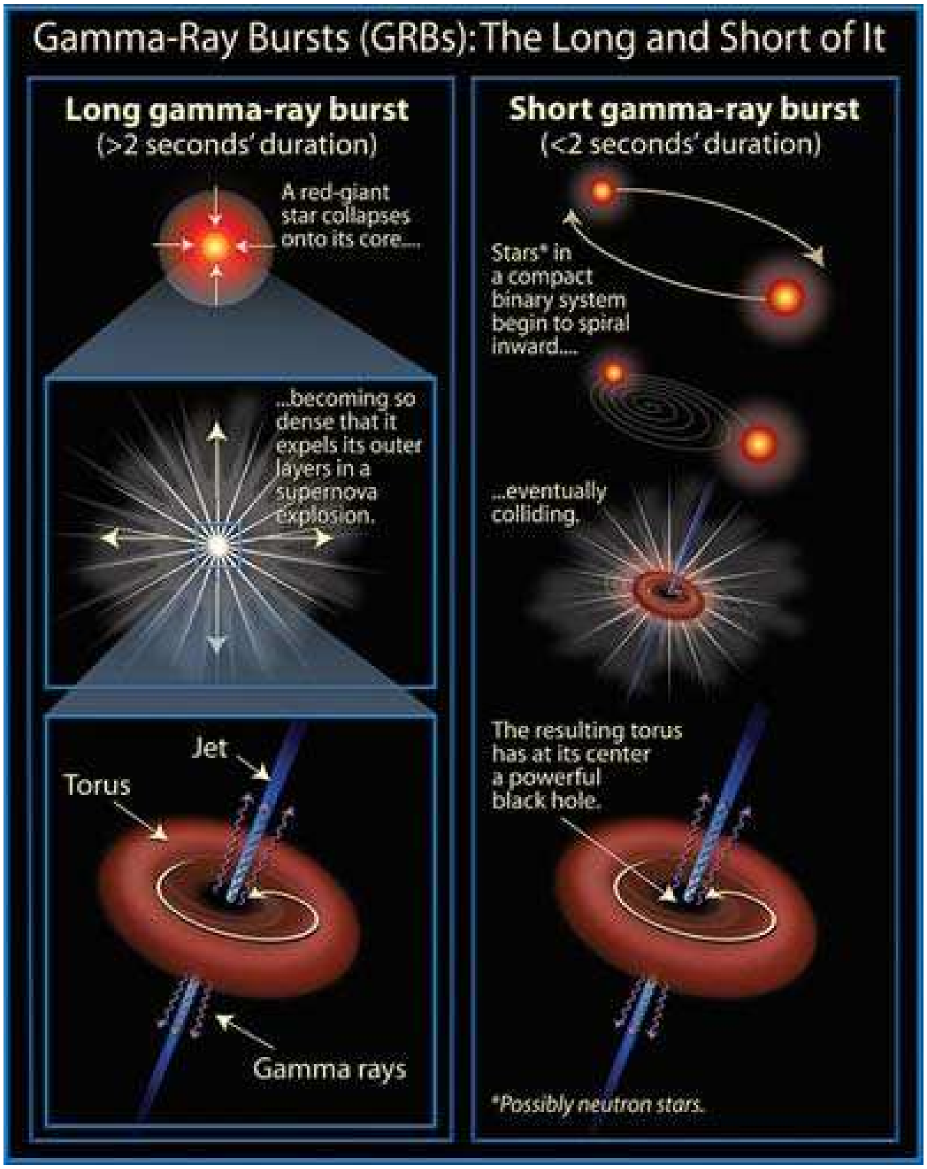

Figure 1.3: Progenitors for long and short gamma-ray bursts. Image courtesy of David Darling.

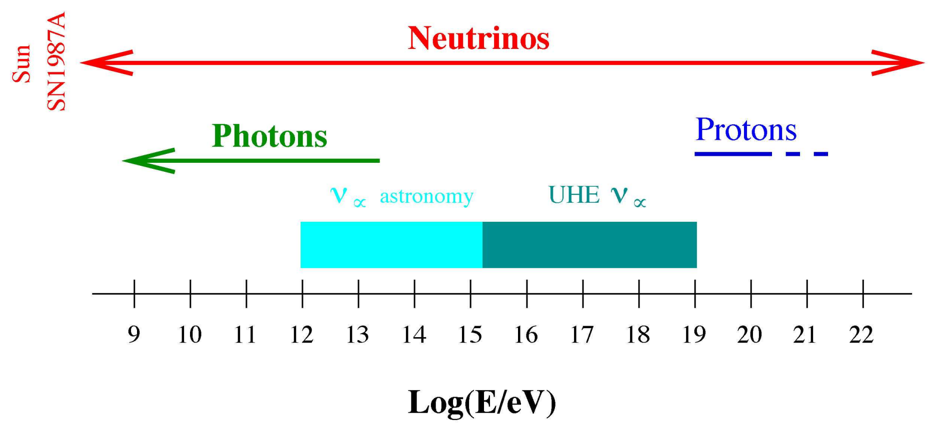

Figure 1.4: Neutrinos open a new window on the universe, allowing observations of environments and phenomena unavailable to us with photons or other particles.

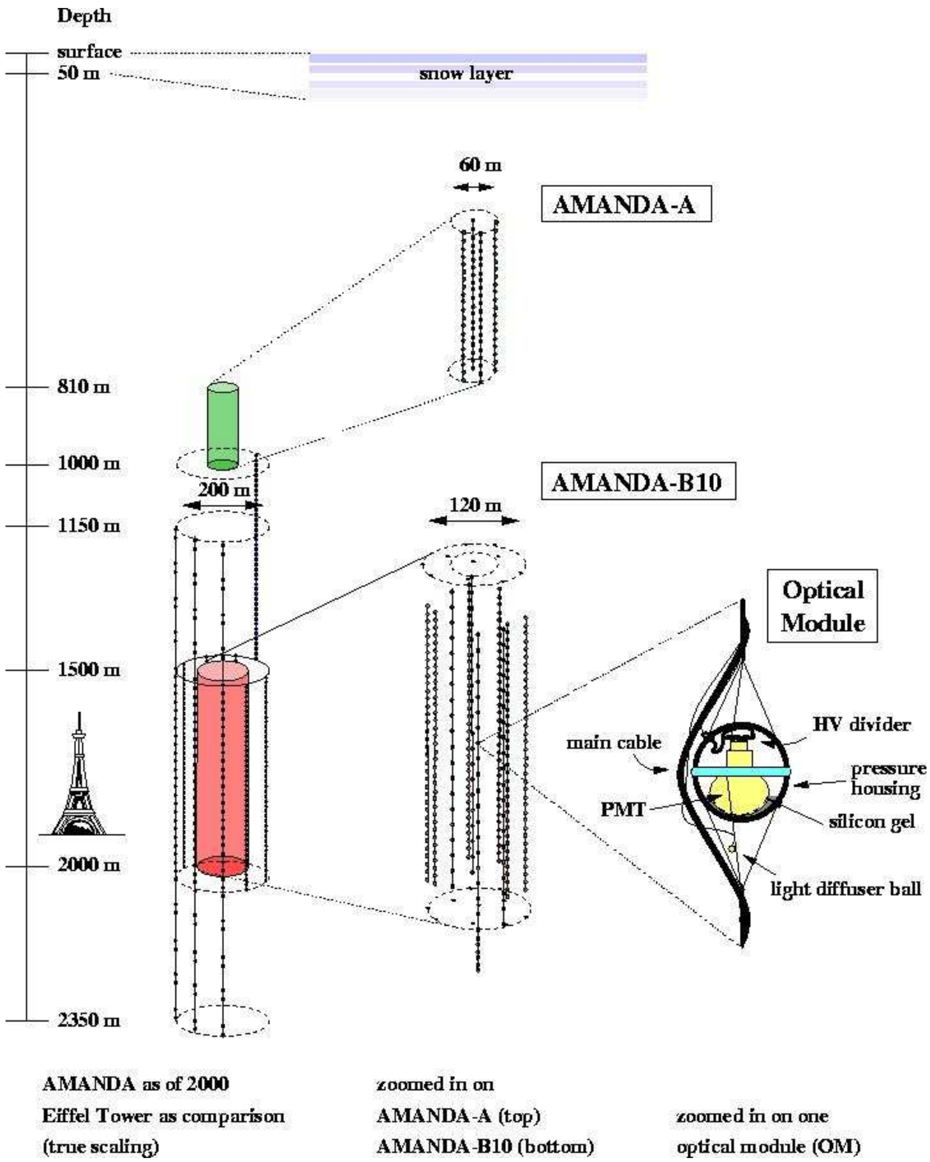

Figure 1.5: The AMANDA Detector, with expanded views of B-10 and a single optical module.

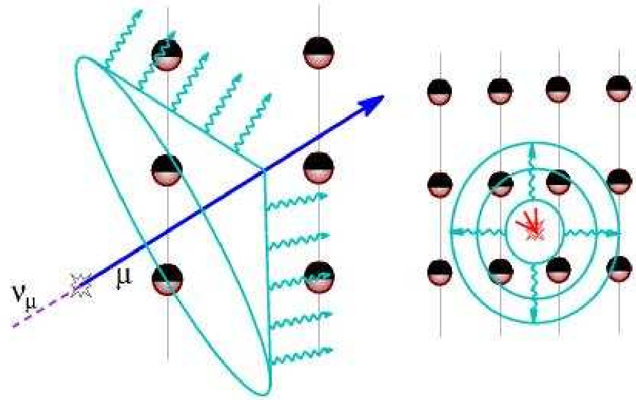

Figure 1.6: Muon neutrinos traveling through the detector are observed by several optical modules as track-like events, which can be used to reconstruct the path of the muons, and thus the direction of origin of the neutrinos (left panel). Events which deposit a significant amount of energy at a single point appear as cascade-like events, with a very different topology compared to tracks (right panel).

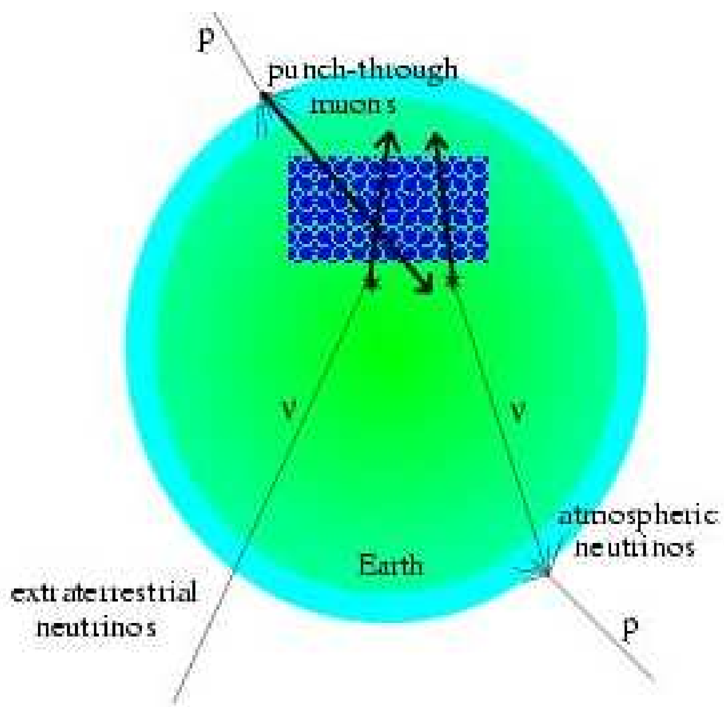

Figure 1.7: Because of downgoing cosmic rays, AMANDA's neutrino signal is drawn primarily from upgoing events, where the background is significantly reduced.

Chapter 2

Models of Neutrino Emission

According to the canonical description provided above, gamma-ray bursts result from the dissipation of the energy of relativistic outflows from a central engine. The source, of radius $\approx 10^7$ cm, produces a jet with an initial luminosity of 10^{52} erg s^{-1}. Most of this radiative energy is transfered to the kinetic energy of the material in the jet, with the Lorentz factor Γ becoming as high as ≈ 300. Variations in the source emission are translated into variations in the kinetic energy of the jet, leading to shocks as the faster material catches up to and interacts with the slower material. Electrons accelerated in these shocks emit synchrotron and inverse-Compton radiation, which is the "prompt" GRB emission. At later times , the wind material will be driven into the interstellar medium, at which point "external" shocks produce the burst afterglow. As described in Chapter 1, the baryonic material within the jet will undergo photopion production, leading to neutrinos that escape the GRB environment.

Based on the assumption that GRBs are the source of ultra-high energy cosmic rays (UHECRs), Waxman and Bahcall predict an annual muon neutrino flux associated with GRBs of $E^2\Phi_\nu \sim 9 \times 10^{-9}$ GeVcm^{-2}s^{-1}sr^{-1} from 100 TeV to 10 PeV (Waxman , 2003) [1]. Murase & Nagataki (2006a) assume a mechanism similar to Waxman and Bahcall for long-duration bursts, though their simulations include a wider range of burst parameters, leading to a wider variation in predicted neutrino fluxes. Inclusion of neutrino oscillations reduce these predictions by a factor of two[2]. Razzaque et al. (2003a) hypothesize a different scenario in which a

[1] For the original formulation of this neutrino flux prediction, see Waxman & Bahcall (1997). Note that this GRB neutrino flux is distinct from the Waxman-Bahcall upper bound on the diffuse neutrino flux due to UHECRs.

[2] Oscillations modify the flavor ratio from 1:2:0 at the source to 1:1:1 at Earth. However, see

supernova precedes a long-duration GRB by several days to a week. In this "supranova" scenario, the supernova remnant provides target photons for p–γ interactions, which will yield muon neutrinos as described above in the standard "fireball" scenario. These neutrinos will be generated up to 10^{16} eV, albeit with a different spectral shape than that predicted by the Waxman-Bahcall version of the fireball scenario[3].

As described in Chapter 1, precursor neutrinos are generated while the GRB jet is still making its way out of the stellar progenitor, and thus are predicted to occur up to 100 seconds prior to the observed photons. Because of the significantly different envirnoment (in terms of particle and photon density, optical depth, and magnetic field strength) these neutrinos have a markedly different energy spectrum compared to the standard "fireball" neutrinos. The precursor model also has implications for gamma-ray dark (or "choked") bursts, which are briefly discussed in Chapter 5.

The "Cannonball" (CB) model of Dar & DeRújula (2001) provides another interesting model capable of being tested by its neutrino predictions. Neutrino observations may be especially important in resolving the dispute between the claims based on photon observations of this model's refutation (Taylor et al. , 2004; Hillas , 2006), and the counter-claims of this model's unparalleled success (Dar , 2006; Dado , 2004; Dar et al. , 2006). The CB model is based on the creation of discontinuous jets of highly relativistic material–the cannonballs. These CBs are caused by discontinuous episodes of accretion of stellar material onto the central compact object formed in the wake of a supernova explosion. The GRB proper is then caused by the interaction of these CBs with the supernova shell.

Kashti & Waxman (2005) for a discussion regarding different flavor ratios due to energy losses of the π and ν.

[3]Though the supranova model is still within the realm of possibility, it is somewhat disfavored based on observations of GRB060218, in which the supernova preceded the GRB by at most a few hours—not long enough to provide an ideal circumburst environment for a significant neutrino flux.

The particle and photon radiation is doppler-shifted and collimated in the forward direction, leading to the observed spectral and temporal behavior associated with all observed GRBs. An enormous number of neutrinos–sufficient for detection above the background even for AMANDA B-10–are expected to be produced for all GRBs with flux above 10^{-5} erg cm^{-2} (about 10% of all bursts). However, the ν emission is beamed even more strongly than the photons (by a factor of 100 in solid angle); thus only 1 in 10^3 observed bursts are expected to have a strong neutrino signal. Therefore, for the CB model we test not the individual burst predictions, but the overall probability of observing neutrinos from any burst within the dataset.

Figure 2.1 shows the expected GRB neutrino flux based on four representative models: the Waxman-Bahcall model, Parameter Set A of the Murase-Nagataki model, the "supranova" model of Razzaque et al., and the precursor prediction of Razzaque et al. For reference, the Waxman-Bahcall "upper bound" is shown (with and without cosmic evolution).

Many theoretical models (most notably, the Waxman-Bahcall model) are based on assumptions regarding the circumburst environment as well as the average properties of bursts (total emission energy, redshift, etc.) which do not correspond directly to the properties of specific bursts. It is possible to estimate the muon neutrino flux for individual bursts, but these estimates vary substantially, and often bracket the predictions of the averaged properties (Stamatikos , 2005; Gupta , 2002). For those bursts where redshift and spectral information is available, more accurate estimates of muon neutrino flux can be made on a burst-by-burst basis. For extremely bright, nearby bursts (e.g. GRB030329), the predicted fluxes can be as much as two orders of magnitude greater than the mean burst flux (Stamatikos , 2006). Furthermore, all of these models (with the exception of Waxman & Bahcall) explicitly incorporate only long-duration bursts into their models, the GRB central engine is in principle independent of burst type. Thus, though the flux upper limits for these models include long bursts only, the models could potentially be expanded to include neutrinos from short bursts as well. Within the AMANDA dataset long bursts dominate over short bursts; incorporating short bursts would have a small, though not insignificant, effect on the overall limit (see Chapter 4 for details). Finally, our simulations assume a Φ_{ν}:$\Phi_{\bar{\nu}}$ ratio of 1:1. AMANDA does not distinguish the muon charge; however, neutrino event rates are larger than anti-neutrino rates for an equal flux, since the neutrino cross section is larger up to energies of $\sim 10^5$ GeV. Thus, any theory that predicts a ratio other than unity will result in a different expected event rate and, ultimately, a different flux upper limit from that presented here.

A wide variety of other calculations of GRB neutrino emission have also been made. Some are based on alternate conditions for the supranova scenario (Dermer & Atoyan , 2003a), or focus specifically on the emission from extremely bright bursts (Dermer & Atoyan , 2006). Dermer & Atoyan (2003b) also determine the expected neutrino emission in the "external shock" model, where the prompt GRB photon emission is created by interactions between the accelerated stellar material and the interstellar medium, rather than "internally", by different shells of accelerated stellar material interacting with one another. This model predicts higher energy ($\approx 10^7$ GeV) neutrinos with a significantly lower peak flux than the Waxman and Bahcall model. Vietri (1998) likewise focuses on the ultra-high energy neutrinos expected from external shocks, though he follows the standard fireball model, where these external shocks produce the GRB afterglow rather than the prompt emission. Finally, DePaolis et al. (2002) predict a significant number of neutrinos from p-nucleon interactions between the GRB-accelerated baryons and a dense circumstellar medium (perhaps generated by the GRB progenitor star's wind). While we do not specifically address these predictions in this work, an observed flux upper limit can be determined for these, or any other, theoretical predictions using the Green's Function method detailed in Chapter 4.

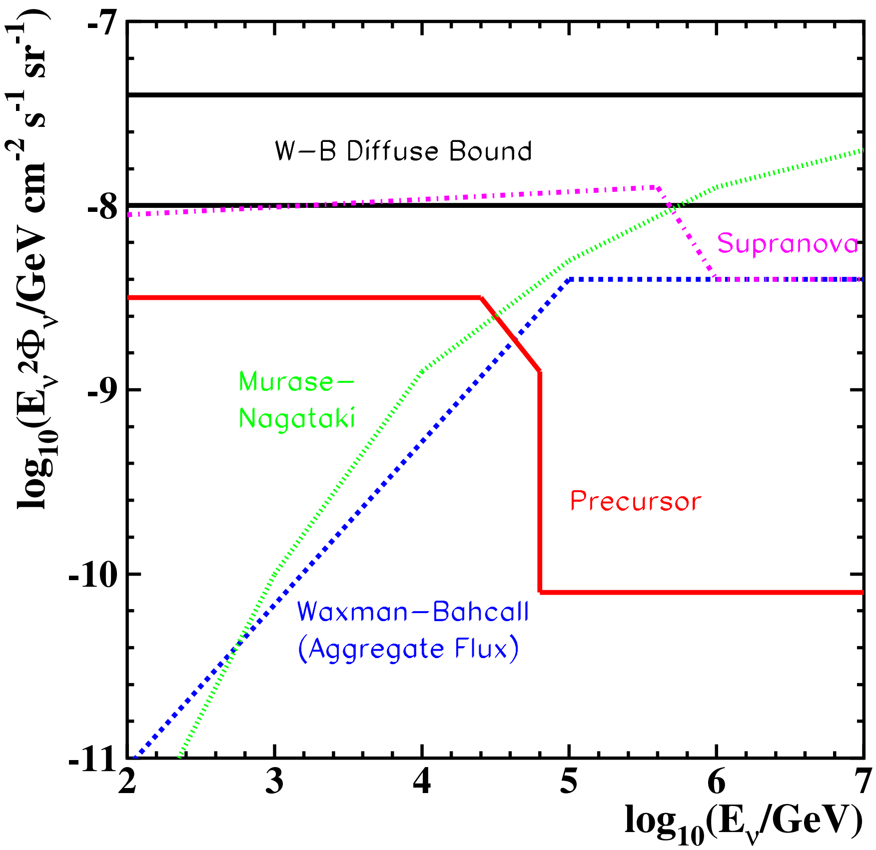

Figure 2.1: Predicted differential muon neutrino flux as a function of energy for four different models of GRB neutrino production: the precursor model (solid line), the canonical Waxman-Bahcall model (thick dotted line), the Murase-Nagataki model (thin dotted line), and the supranova model (dot-dashed line). All models include the effect of ν oscillations. The diffuse neutrino bounds determined from cosmic ray observations with (upper horizontal line) and without (lower horizontal line) z evolution are also shown for reference.

Chapter 3

Observation Procedure

3.1 Correlated Observations

This AMANDA GRB search relies on spatial and temporal correlations with photon observations of other instruments including BATSE aboard the Compton Gamma-Ray Observatory (CGRO), as well as HETE-II, Ulysses, and other satellites of the Third Interplanetary Network (IPN) (Hurley , 1998). As stated previously, our search is restricted to that half of the bursts occurring in the Northern Hemisphere. Furthermore, because engineering and maintenance work is performed on the AMANDA detector during the austral summer (December-February), only a few bursts from these months can potentially be observed each year. For each GRB in the dataset, we search for muon neutrino emission during the coincident phase of burst emission. The coincident phase is determined by either the T_{90} start and end times of the burst, or the entire duration of emission in excess of the background rate (for bursts without well-defined T_{90}). A period of time before and after each burst is added to the search in order to accommodate the timing errors of the photon observations (which vary from burst to burst). Most bursts have prompt phases lasting from a few seconds up to to a few tens of seconds, though there are some exceptional bursts lasting hundreds of seconds. To investigate different model predictions for the bursts occurring during 2001-2003, we also performed an extended search for precursor neutrinos from 110 seconds before the burst start time until the beginning of the coincident search window. BATSE observations were the sole source of data for the AMANDA B-10 analysis for 1997–1999. Other IPN-detected bursts were included beginning with the AMANDA-II dataset in 2000, and the analysis then relied exclusively on IPN data from other satellites once CGRO was decommissioned in May, 2000.

A number of BATSE non-triggered bursts were are also incorporated into this analysis. Because these bursts had significantly lower photon flux compared to the standard bursts, they did not reach BATSE's on-board detection threshold; however, they were detected in subsequent off-line searches of BATSE's archival data (Kommers , 1998; Stern et al. , 2001). Though the lower photon flux of these bursts is assumed to correspond to a lower neutrino flux, the relevant time periods of the AMANDA data were searched for muon neutrinos from these bursts as well. We do not, however, include this particular subset of bursts in the flux or fluence upper limits for the models addressed in this work, because non-triggered bursts were not incorporated into the primary models of GRB neutrino emission (see Section 3.4 for further details).

The instruments participating in the Interplanetary Network through 2003 are given in Table 3.1 and the number of bursts searched in each year of AMANDA observations is listed in Table 3.2. Information on the specific bursts included in this analysis is given in Table 3.3.

3.2 Background and Detector Stability

To determine the background rate and to establish data selection criteria for each burst, a larger period of one hour and 50 minutes of data is analyzed—from one hour before the burst to one hour after the burst, with the 10 minute period during and immediately surrounding the burst excluded to ensure that the data quality cuts are not determined in a biased fashion (a "blind" analysis, see Figure 3.1). Prior to determination of the data selection criteria, we study detector stability in this background period. The specific stability criteria for AMANDA B-10 have been discussed previously (Hardtke , 2002); here we describe the AMANDA-II stability criteria in more detail.

We perform two tests to identify non-statistical fluctuations in the data rate that could produce fake events ("false positives") or unanticipated dead time ("false negatives") in the detector. The first test compares the observed event count per 10 second time bin to the expected, temporally uncorrelated, distribution of background events. This tests for any non-statistical fluctuations in data rate due to temporary instability in the detector. Without this test, an upward fluctuation in the data rate not caused by neutrinos could potentially be misinterpreted as a signal event. This test has three successive steps based on the P-value of the event rate distribution. The P-value of a data segment is defined as the percent difference between the RMS variation of the data event rate and the width of a Gaussian fit to the data rate distribution. The first step identifies all those bursts with stable periods—those having a P-value of less than 6% (corresponding to variations of less than 1σ relative to the overall distribution of P-values). The second step identifies bursts with marginally stable detector performance: 6%≤P≤12% (1–2σ). Additional tests are performed on these bursts; specifically, the data rate of the previously blinded 10-minute period is explored in a region of the sky far away from the GRB (the "on-time, off-source" region). This maintains the blindness of the analysis, while allowing a more detailed exploration of detector stability. Marginally stable burst periods are included in the analysis if they are also marginally stable in the on-time, off-source region (P-value less than 12%), and if the event rate has only small (≤3σ) variations throughout the on-time, off-source region. The vast majority of all burst time periods were stable according to these criteria. The final step of this test is applied if the first two steps are inconclusive. It requires any event rate variations greater than 3σ to occur at a significant distance from the burst time. Two bursts fall into this category; they had marginally stable off-time periods and insufficient statistics for an on-time/off-source stability test. However they were included in this analysis because the largest event rate variations were separated in time from the burst by several minutes. Only one time period associated with a burst in the AMANDA dataset had off-time and on-time/off-source P-values greater than 12%, and this burst was excluded from the analysis. Figure 3.2 shows the data rate per 10 seconds for a sample GRB period, overlaid with the Gaussian fit. They are in very good agreement, showing a stable data rate for this period of detector activity.

The second test utilizes the time between subsequent events (δt) to ensure that there is not an anomalously large amount of time between detector triggers. The amount of time between triggers can vary widely, but larger gaps occur with much less frequency than shorter gaps. There is also unavoidable (but quantifiable) dead time between each trigger while the detector is being read out. The overall effect of the expected dead time is to reduce the detector's signal acceptance by approximately 17%, and this quantity has been incorporated into the expected neutrino observation rate for this analysis. However, large unexpected gaps between triggers would indicate a period of unstable detector performance, and would mean that an otherwise detectable neutrino signal might not be observed during such a period. We test the 1 hour and 50 minute time periods surrounding each burst to ensure that no such gaps occur. An example of the temporal distribution of triggers compared with an exponentially decreasing fit to the δt distribution is shown in Figure 3.3. The variations observed in the data for this time period are within 2σ of the observed fit for all values of δt. Thus there are no unexpected variations in the time between detector triggers, and we confirm that AMANDA is collecting data as expected occurring during the on-time window for this burst. All data periods associated with GRBs that pass the first test also pass this second test for stable detector operation.

3.3 Data Selection Criteria

For those bursts determined to be stable by the above criteria, data quality cuts are then selected to separate the predicted signal from the observed background events. This process relies primarily on the simulated signal events and the observed background events. The simulation of the detector response to signal and background events is described in Ahrens et al. (2004). The simulation procedure uses the neutrino generation program NuSim (Hill , 1997) (and occasionally the muon generation program muo0) for signal event simulations. Background events are simulated with CORSIKA (Heck et al. , 1998), which implements the 2001 version of the QGSJET model of hadronic interactions (Kalmykov & Ostapchenko , 1993). Once the neutrino or other cosmic-ray primaries are generated and propagated to their interaction vertex, we simulate the secondary propagation with the Muon Monte Carlo (MMC) package (Chirkin & Rhode , 2004). Finally, we simulate the AMANDA detector response with the software package AMASIM. We then are able to compare simulated signal, simulated background, and observed background data.

In the case of the GRB search, the background rate is measured using the off-time window, where no signal is expected. Thus, unlike other AMANDA analyses (Ahrens et al. , 2003a,b), the background events do not need to be simulated, nor do the data events need to be scrambled in time or azimuth to retain a blind analysis procedure. Exploring the variations between observed background events and simulated events does, however, ensure that we understand the systematic errors associated with the simulation process. For example, Figure 3.4 shows excellent agreement in $\mathcal{L}_{reco}$, the log(Likelihood) of the reconstructed tracks of the simulated and observed background events. Given this level of agreement, the errors arising from discrepancies between the simulated and observed events are expected to be small. Additionally, atmospheric neutrinos have previously been observed by AMANDA up to TeV energies, and studies show that neutrinos from this proven source can be reconstructed with a high degree of accuracy (Andrés et al. , 2001). Likewise, studies have been performed which compare simulated signal events with high-quality downgoing muon events (Hodges , 2006). Because these downgoing events have similar properties to the simulated signal events, this provides additional assurance that the simulated signal events will have similar properties to the actual signal events we are attempting to observe. Section 3.4 gives a quantitative discussion of systematic errors.

To determine the set of data selection criteria that will produce the optimal flux upper limit in the absence of a signal, we minimize the Model Rejection Factor (MRF) (Hill & Rawlins , 2003). The MRF is based on the expected detector sensitivity prior to observations:

$$MRF = \frac{\bar{\mu}_{90}(\mathrm{N}_{\mathrm{BG,Exp}})}{\mathrm{N}_{\mathrm{Sig}}} \tag{3.1}$$

where $\bar{\mu}_{90}$ is the Feldman-Cousins 90% average event upper limit (Feldman & Cousins , 1998) derived from the expected number of background events ($\mathrm{N}_{\mathrm{BG,Exp}}$) and $\mathrm{N}_{\mathrm{Sig}}$ is the expected number of signal events. $\mathrm{N}_{\mathrm{Sig}}$ is determined by convolving the theoretical spectrum ($\Phi = \mathrm{dN}_\nu/\mathrm{dE}$) with the detector's energy- and angle-dependent effective neutrino collecting area ($A_{eff,\nu}$) and integrating over the angular acceptance of the detector, the energy range of interest (10^2 to 10^7 GeV), and the observation time (assuming 700 bursts contribute equally to the annual expected flux):

$$N_{\mathrm{Sig}} = \int\int \Phi(E, \theta, \phi) A_{\mathrm{eff},\nu}(E, \theta) \mathrm{dEd\Omega dt}. \tag{3.2}$$

As an intermediate step in the determination of the expected number of signal events, we therefore need to determine the detector effective collection area. $A_{\mathrm{eff},\nu}$ is determined by the fraction of simulated neutrino events that are retained after all data selection criteria are applied. This area also accounts for neutrinos that generate muons passing nearby (but not through) the detector and still cause the telescope to trigger.

In determining the optimal data selection criteria for the coincident search, we assume a Waxman-Bahcall neutrino spectrum (Waxman , 2003); for the precursor search, we assume a Razzaque spectrum (Razzaque et al. , 2003a). In addition to temporal coincidence described previously, the most relevant selection criterion for this analysis is the angular mismatch ($\Delta\Psi_{\mathrm{i}}$) between the burst position and the reconstructed event track. This mismatch is determined for each of four separate maximum-likelihood pattern recognition algorithms (i = 1 to 4) applied to the timing of the hit OMs (as described in Chapter 2). The different algorithms are based on different initial seeds and apply a different number of iterations to the track reconstruction procedure, thus they are able to provide different measures used for discrimination between expected signal and background events. The reconstruction algorithms applied include the "direct walk" fit and the single-iteration pandel fit, as well as the 16- and 32-fold iterative pandel fits. The pandel function is defined as

$$p(t) = \frac{1}{N(d)} \frac{\tau^{-(d/\lambda)} t^{(d/\lambda - 1)}}{\Gamma(d/\lambda)} e^{-(t(\frac{1}{\tau} + \frac{\bar{c}}{\lambda}{}_a) + \frac{d}{\lambda_a})} \tag{3.3}$$

where the normalizaton factor

$$N(d) = e^{-d/\lambda_a}(1 + \frac{\tau\bar{c}}{\lambda_a})^{-d/\lambda}, \tag{3.4}$$

t is the difference between the observed hit time and the hit time expected for a direct (unscattered) photon, $\bar{c}$ is the speed of light in ice, λ_a is the absorption length, $\Gamma(d/\lambda)$ is the gamma function, and λ and τ are free parameters based on the geometry of the detector and determined by Monte Carlo simulations.

Though the individual reconstruction algorithms are not completely independent, they do offer improvements to the MRF when applied consecutively. The inherent difference in the muon and neutrino paths, as well as the inaccuracies of the reconstruction algorithms, prevent perfect characterization of all signal and background events. Nevertheless, the angular mismatch is quite effective as a selection criterion. For example, selecting events with a mismatch angle $\Delta\Psi_1$ of less than 12° retains more than 90% of the expected signal events, while reducing the background to less than 0.5% (Figure 3.5). Depending upon the changes in the detector characteristics and the analysis tools from year to year, the MRF optimization procedure allowed for some variation in the specific track reconstruction algorithms applied, as well as the mismatch angle values selected for each algorithm (see Table 3.4).

Several secondary criteria were also used to improve the separation between signal and background events. Included in the secondary criteria is the measured number of hit channels—that is, the number of OMs participating in the reconstruction of each event. The number of direct hits—hits that occur within -15/+75 ns of the arrival time for light propagating from the reconstructed muon track to the OM in question—also serves as a useful criterion for data selection. Direct hits should be due to photons that do not scatter, or scatter minimally; their straight trajectories give them a well-defined behavior, making them most useful in determining the muon direction. Additionally, the likelihood of a given reconstruction and the angular resolution (σ_Ψ) of the alternate event track reconstruction (the "paraboloid fit") provide a useful event discriminator, since high quality signal events will have higher likelihoods and superior angular resolution compared to the background events. One additional criterion used in this analysis is the uniformity of the spatial distribution of the hit OMs—events with hit OMs spread evenly along the track are more likely to be single high-energy neutrino-induced muons, whereas events with hit OMs clustered in time and space along the track are more likely to be background events. Different combinations of these criteria were applied in the 1997-1999, 2000, and 2001-2003 timeframes, as new analysis tools were developed and applied to the GRB neutrino search (see Table 3.4).

This analysis procedure was applied to bursts with localization errors from the satellite observations that are relatively small (typically less than 1°) and therefore inconsequential on the scale of the AMANDA search bin radius. However, several hundred IPN bursts have large localization errors (≥1/2 of the search bin radius), but still lie completely within the field of view of AMANDA. These were either marginal detections near the edge of BATSE's field of view or they were detected by only two IPN satellites without directional sensitivity, which prevents triangulation of their position but allows localization to an annular segment based on relative timing considerations (Figure 3.6). Eleven of the bursts in this dataset are only poorly localized; the increased search area for these bursts results in a corresponding increase in the expected background rate[1]. To ensure that this increase does not diminish the overall sensitivity of the GRB search, more restrictive selection criteria are applied to these bursts. Whether well localized or

[1] Analysis of an additional 54 poorly-localized bursts from 2001-2004 has been performed, with the results to be forthcoming (Frankcowiak , 2007)

poorly localized, each burst has an associated background expected during the burst time, calculated from the event rate of the off-time background region multiplied by the duration of the time window during which we search for signal events.

The initial criteria were independently selected to optimize the MRF and were then collectively optimized in an iterative fashion. The optimal criteria depended on the zenith angle of the burst, due to the higher observed background rate for bursts closer to the horizon. The criteria for higher background rates (i.e. low zenith angle bursts) were also applied to bursts with large satellite localization errors, regardless of the actual zenith angle of the burst. Table 3.4 lists all data selection criteria used for the year-by-year GRB analyses, as well as the selection criteria for the precursor search applied in 2001-2003. Figures 3.7 through 3.16 show a comparison between simulated signal and observed background events for various selection criteria from the 2000 and 2001-2003 analyses. Though these criteria are optimized for specific models of neutrino emission, other models can also be tested using the Green's Function Fluence Limit Method (see Results). While the muon track reconstruction algorithm is very accurate, there is a small probability that a downgoing muon will be misreconstructed in the upgoing direction; such events are the primary background for the GRB search. After the application of data selection criteria, background events have an observed rate of $\sim 5\times 10^{-5}$Hz (with some seasonal variation).

A determination of the relative MRF for a subset of bursts from the year 2000 analysis is shown in Figure 3.17 (the arrow indicates the relative MRF for the selected criteria). Figure 3.18 shows the effective area for neutrinos for the AMANDA-II detector after all data selection criteria are applied. Due to the large instrumented area and modest background rejection requirements of this analysis, AMANDA-II has an A_{eff} significantly larger than any other contemporaneously-operating neutrino detector (e.g. Baikal (Spiering et al. , 2004), SuperKamiokande (Fukuda et al. , 2002), and SNO (Aharmim et al. , 2000)).

Prior to "unblinding" the analysis and determining the number of events we observe, we determine the flux sensitivity to simulated GRB neutrinos. Results from the 268 bursts observed from 1997 to 1999 have been presented previously (Bay , 2000; Hardtke , 2002). We combine these initial observations with the results from the analysis of 151 bursts in the data collected in 2000-2003. The number of expected signal events for various theoretical models is calculated according to Equation 3.2 and is given in Table 3.4. The flux sensitivity for all 419 bursts is the MRF prior to observations (see equation 3.1) multiplied by the normalization of the input spectrum; that is, $E^2\Phi_\nu \leq 2 \times 10^{-8}$ GeVcm^{-2}s^{-1}sr^{-1} for a Waxman-Bahcall muon neutrino spectrum with 90% of the events expected between ~10 TeV and ~3 PeV. This sensitivity is calculated prior to the inclusion of systematic uncertainties.

3.4 Uncertainties in Observation and Modeling

There are several potential sources of systematic uncertainty in this analysis, including the Monte Carlo simulations of signal events, the modeling of the scattering and absorption lengths of the South Pole ice, and the OM response to incident photons. For the flux upper limits incorporating IPN bursts, the potential for inclusion of bursts which do not fit models based upon BATSE triggered bursts contributes to the overall uncertainty as well. Additionally, some bursts are of unknown duration–for the purposes of this search, they were classified as long-duration bursts so that we would not needlessly exclude any possible signal events. However, including all such bursts will potentially overestimate the signal event predictions for models based solely upon long-duration bursts.

Finally, previous results from 1997-1999 were applied only to the Waxman-Bahcall model; limitations in the simulation procedures in place at that time means that adapting these results to other models will introduce uncertainties in the expected neutrino event rate.

The scattering and absorption lengths of the ice were measured during the 1999-2000 austral summer with in situ lasers and LED flashers (Ackermann et al. , 2006). While these measurements were extremely accurate, the limited precision with which they were implemented in our detector simulations contributes about 15% to the overall uncertainty. Furthermore, the quantum efficiency of the photomultiplier tubes is known to within 10%, while the transmission efficiency of the glass pressure housing and the optical gel is known to a comparable precision. However, triggering depends on the detection of photons by 24 or more PMTs, so the uncertainty in a single OM does not translate directly into an uncertainty in the expected flux. Detailed simulations show that the quantum and transmission efficiencies together contribute only about 7% uncertainty in the expected neutrino flux (Ahrens et al. , 2004). Though the GRB search implements a different methodology from other IceCube analyses (e.g. the point source search detailed in Achterberg et al. , 2006b), the values for the individual contributions to the uncertainty are consistent across these different analyses.

Additionally, a statistical correction is required when IPN bursts are incorporated into the flux upper limits for models initially based on BATSE observations. In principle, BATSE has a sensitivity comparable to the suite of other IPN satellites treated collectively; observationally, their duration distribution seems qualitatively to be derived from the same bimodal population (Figure 3.19). However, the characteristics of the bursts detected by satellites with different sensitivities are not completely identical. BATSE non-triggered bursts have on average 1/20 of the peak photon flux of their triggered counterparts (see

Figure 3.20), and if we assume that the neutrino flux scales as the photon flux, then including non-triggered bursts in the upper limit calculation would artificially increase the expected number of signal events, and thus lead to a flux upper limit that is too restrictive. We calculate (see Appendix A) that 12% of the IPN bursts should not be considered equivalent to BATSE triggered bursts, and thus should be excluded from the dataset. This leads to a 3% correction in the number of expected signal events. Furthermore, for models based solely on long-duration bursts such as Murase & Nagataki (2006a); Razzaque et al. (2003a), the inclusion of bursts of unknown duration may also lead to an overestimation of the number of expected signal events. In Appendix A, we derive a statistical correction of 6% to the expected number of signal events due to this effect.

Finally, we determine the uncertainty introduced when the previous results from 1997-1999 are applied to theoretical predictions other than the Waxman-Bahcall model. Though the uncertainties specifically for the Waxman-Bahcall model are well understood and are incorporated into the previous results, limitations in the simulation procedures at the time of the previous analysis lead to a further uncertainty in the neutrino event rate for the Murase-Nagataki and Razzaque et al. models of $\sim$20%. When we combine the results from the 268 bursts from 1997-1999 with the results from 151 bursts from 2000-2003 into a single flux upper limit, we assume conservatively that the neutrino event rate for the bursts from 1997-1999 is overestimated by 20%.

All significant sources of uncertainty for the GRB analysis, along with the correction factors, are summarized in Table 3.5. While the reduction in the expected neutrino event rate for the 1997-199 bursts is not specifically enumerated in this Table, it is incorporated into the relevant flux upper limits discussed in the next chapter. Assuming no correlation among the other uncertainties, we summed the different factors in quadrature and applied the other relevant corrections to obtain a total uncertainty of +16%/-17% (+15%/-18% for models based on long-duration bursts only) in the total detector exposure, and therefore in the number of signal events and the flux and fluence upper limits. This is comparable to the uncertainty determined by Hodges (2006), who also characterized the agreement between the simulated signal events and high-quality downgoing muon events, which served as a proxy for the expected signal events for AMANDA analyses.

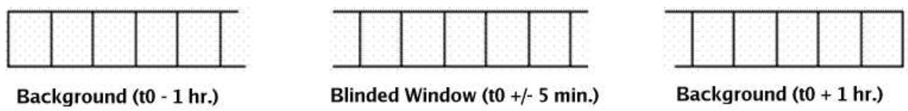

Figure 3.1: A schematic representation of the on-time and background regions for each GRB.

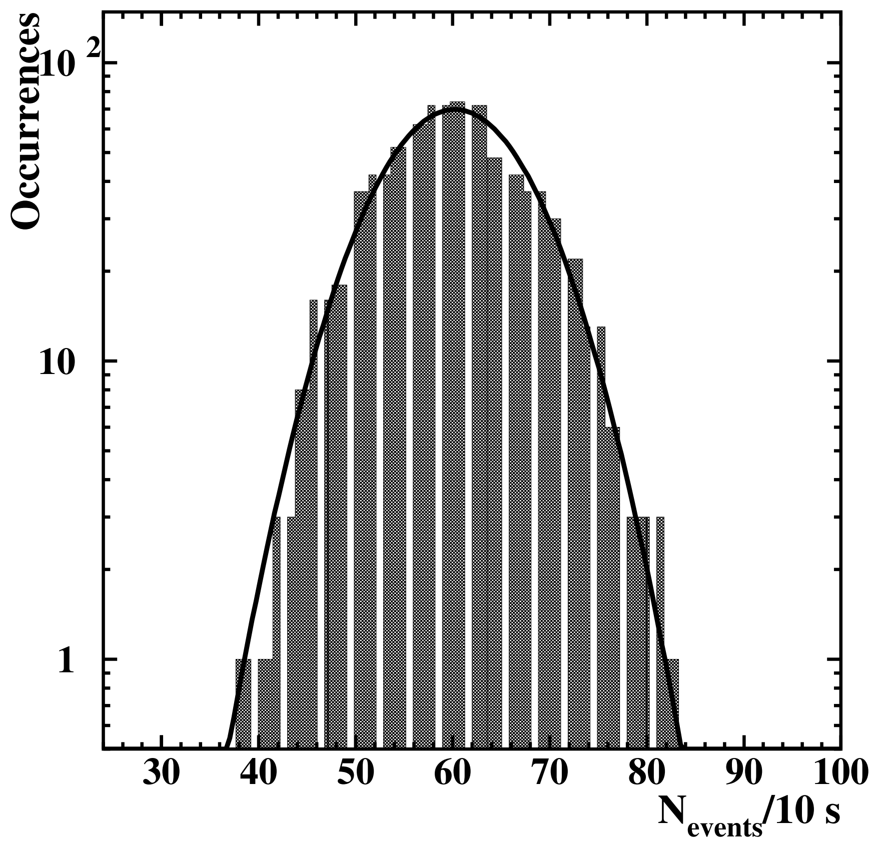

Figure 3.2: A stable period of detector activity, shown by the nearly Gaussian random temporal distribution of events in each 10-second bin during the off-time period of a representative burst. Initial selection criteria have been applied to these data, but the GRB-specific criteria have not yet been applied.

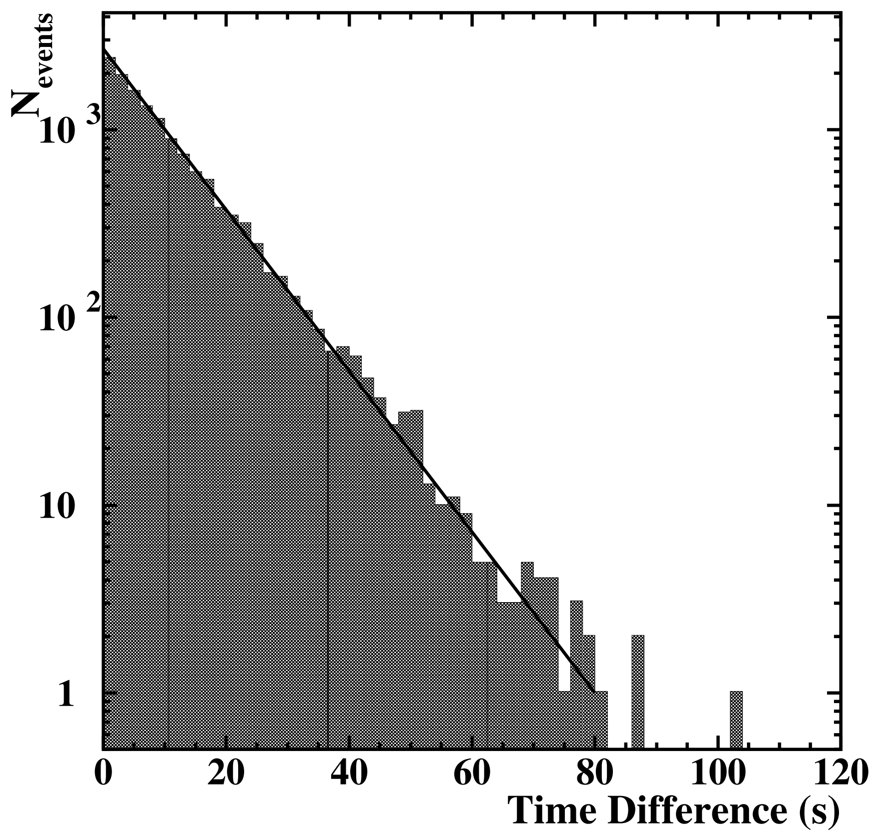

Figure 3.3: Time difference (δt) between subsequent events during the background time period of a representative GRB, after application of initial data quality cuts. There is no evidence for significant gaps in the data that could produce a "false negative" result.

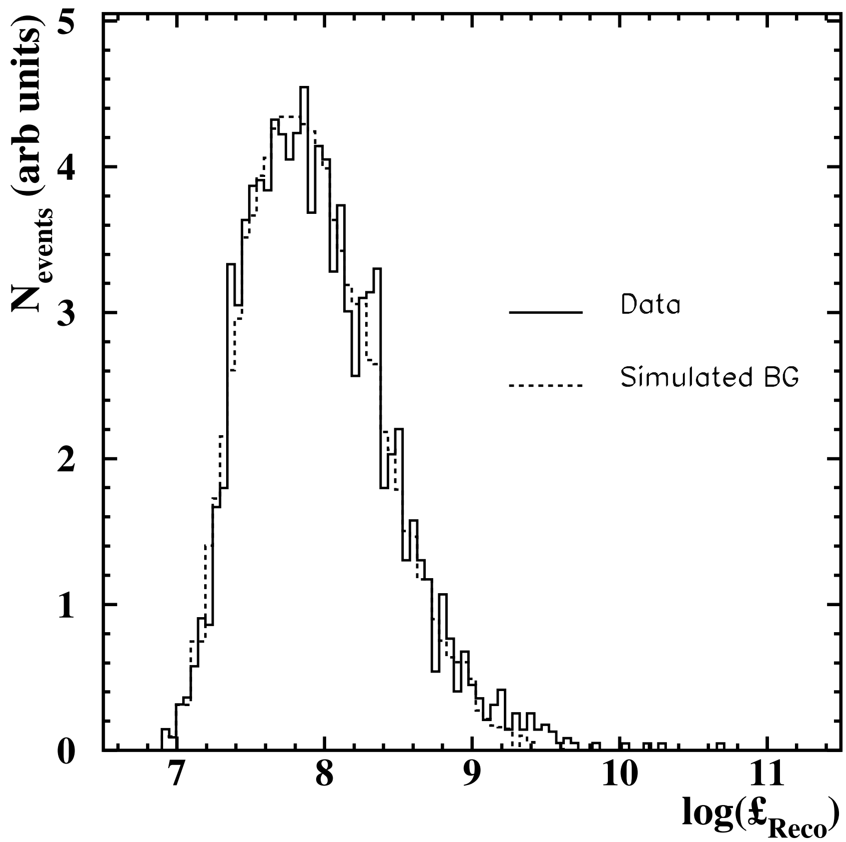

Figure 3.4: A comparison of the likelihood of track reconstruction, £$_{reco}$ for observed data (solid line) and simulated background events (dashed line). Both curves are normalized after preliminary data selection criteria are applied. The close agreement signifies that our simulations are properly modeling the observed events, thus providing additional evidence for the trustworthiness of the simulated signal events as well.

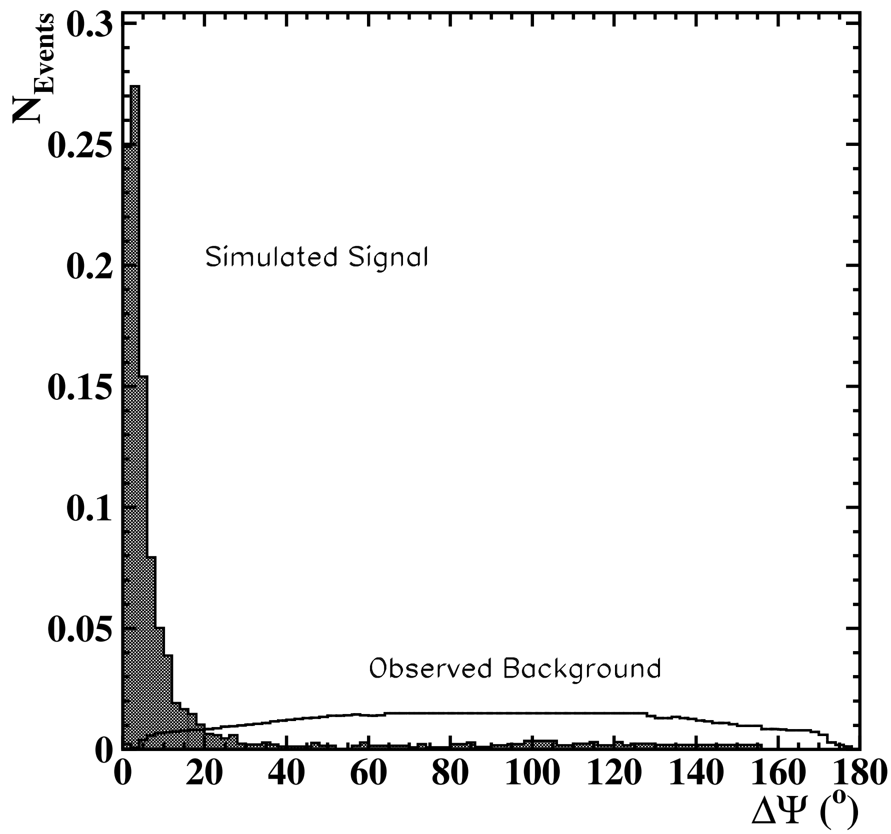

Figure 3.5: The expected distribution of angular mismatch $\Delta\Psi_1$ for a simulated muon neutrino spectrum (shaded region) and observed background (open region). $\Delta\Psi_1 = 0$ is the position of the burst determined from photon observations. Selecting events with $\Delta\Psi_1 \leq 12°$ retains more than 90% of the signal events.

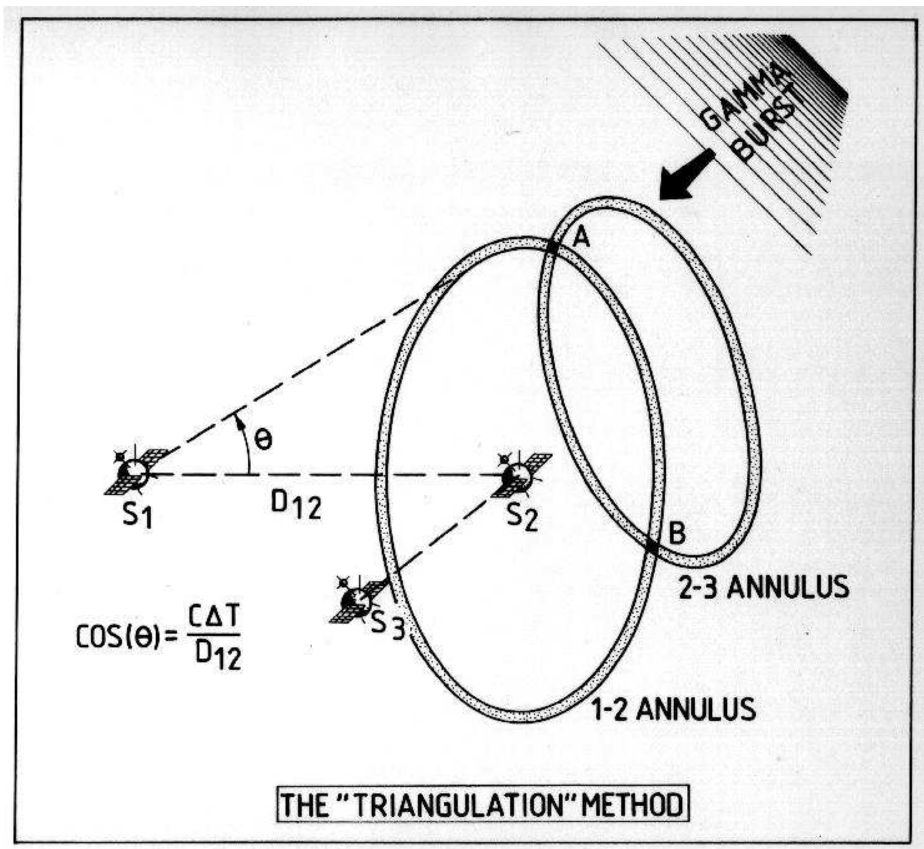

Figure 3.6: Schematic depiction of annular localization of a gamma-ray burst by the satellites of the InterPlanetary Network.

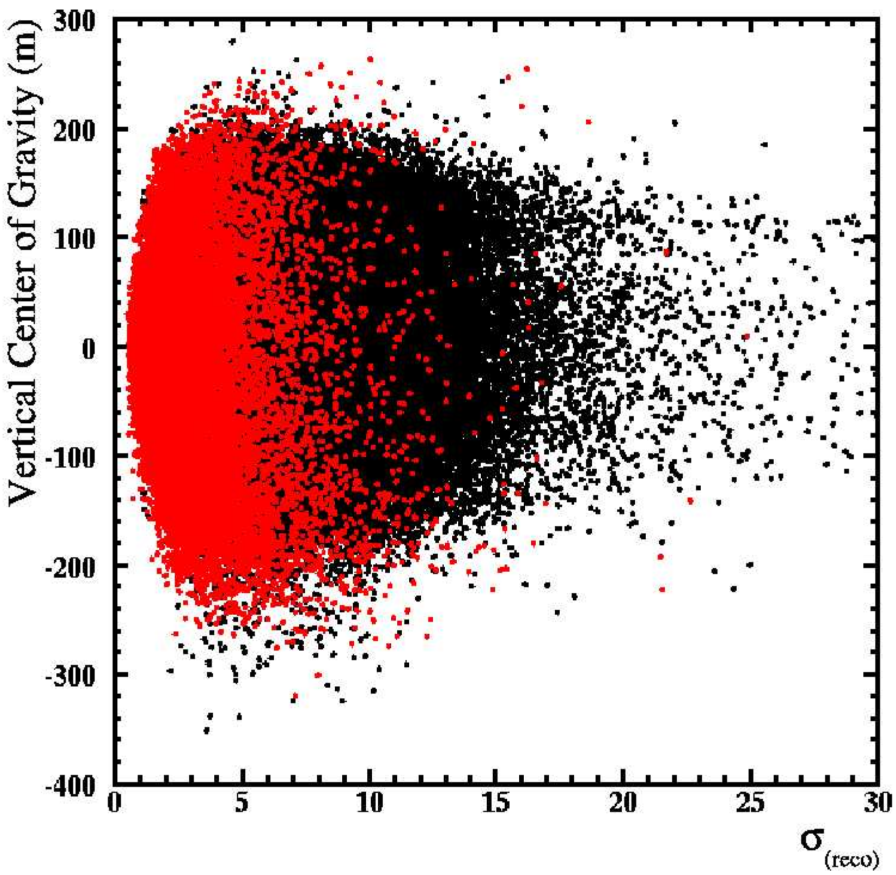

Figure 3.7: Vertical Center of Gravity of Hits vs. Angular Resolution (σ_{reco}) of the paraboloid fit, for simulated signal (red) and observed background (black).

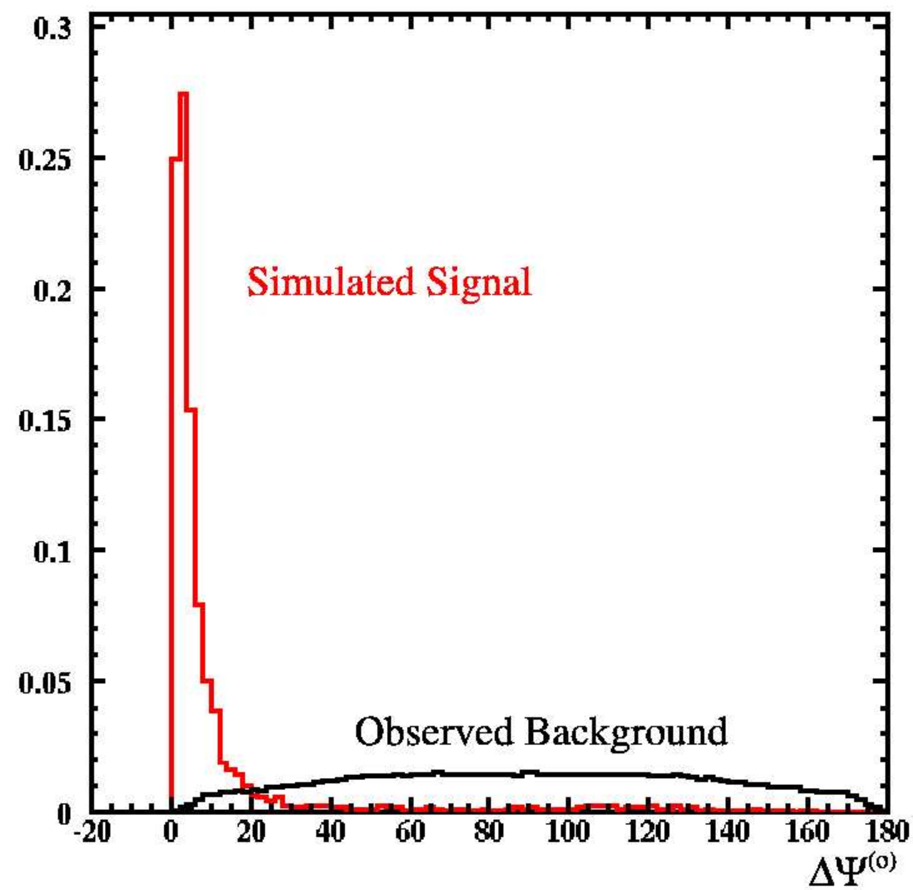

Figure 3.8: Spaceangle distribution for 16-fold iterative pandel mpe fit for simulated signal (red) and observed background (black) events.

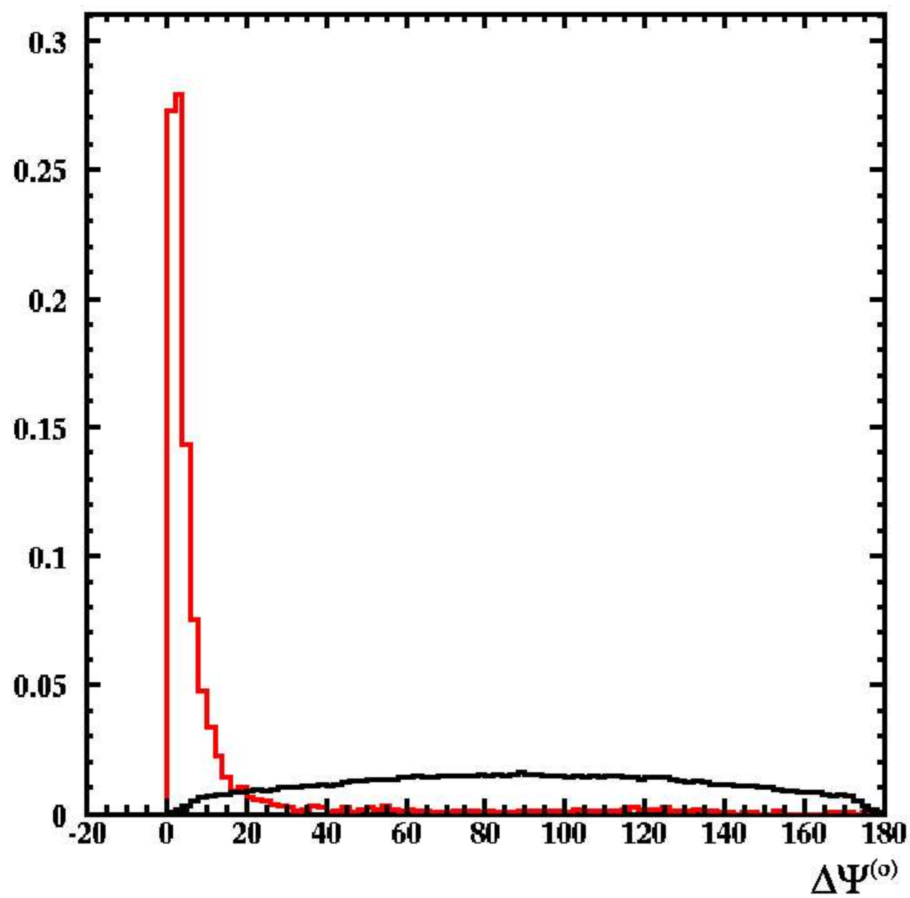

Figure 3.9: Spaceangle distribution for single-iteration pandel fit for simulated signal (red) and observed background (black) events.

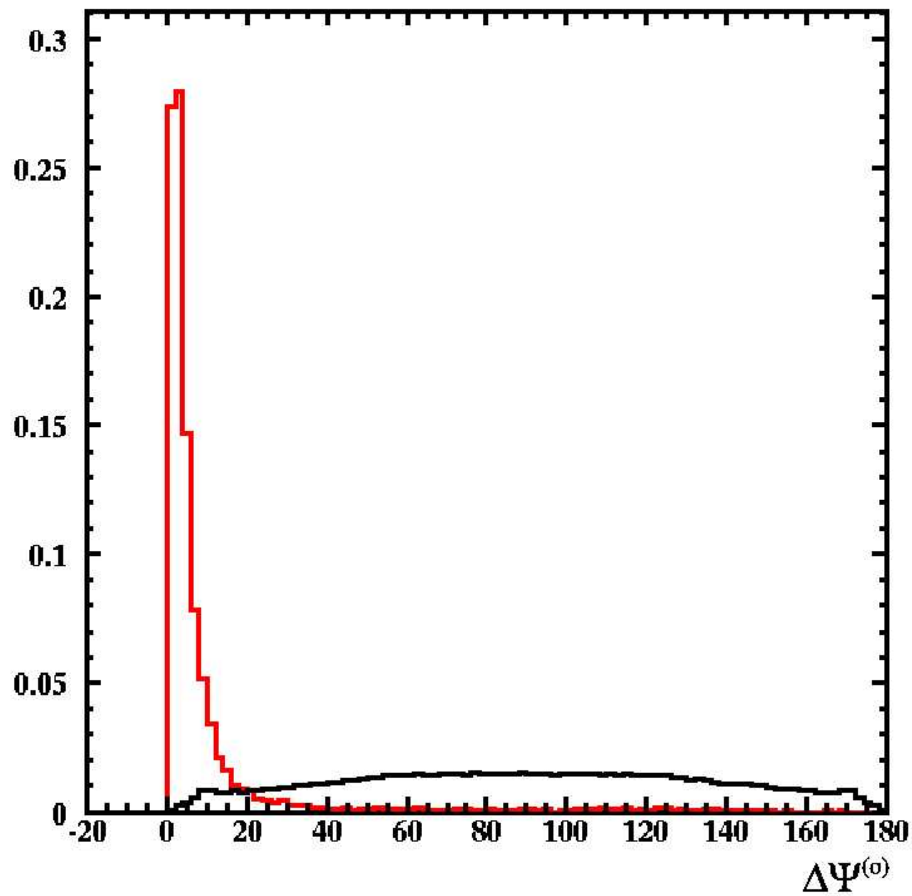

Figure 3.10: Spaceangle distribution for 32-fold iterative pandel fit for simulated signal (red) and observed background (black) events.

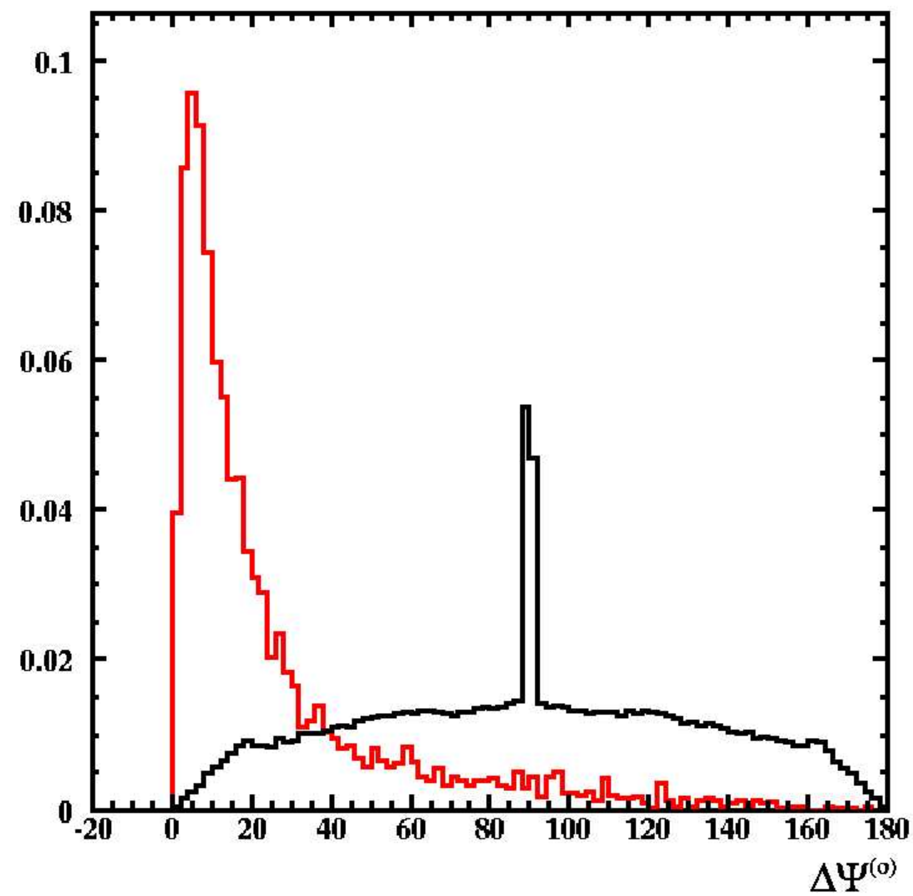

Figure 3.11: Spaceangle distribution for direct walk fit for simulated signal (red) and observed background (black) events. The spike in the background distribution is due to low-quality events that do are not successfully reconstructed.

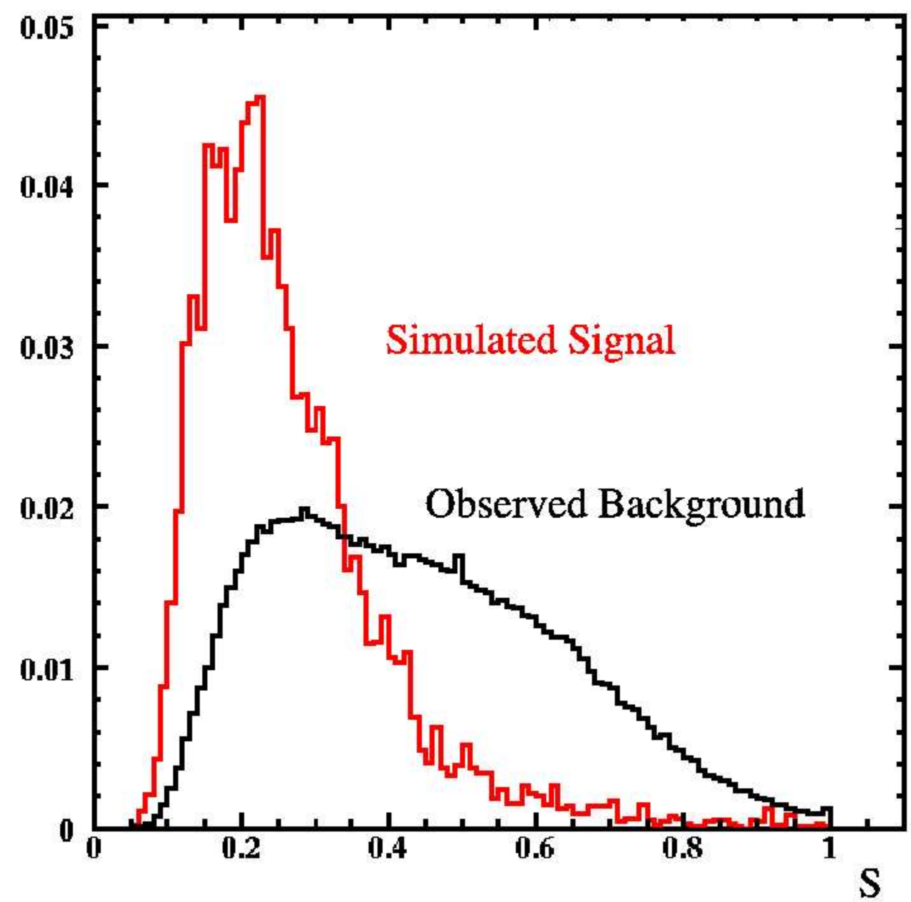

Figure 3.12: Smoothness distribution for 2001-2003 analysis. Simulated signal events (01-03 MC) are red and observed background events (2003 data) are black.

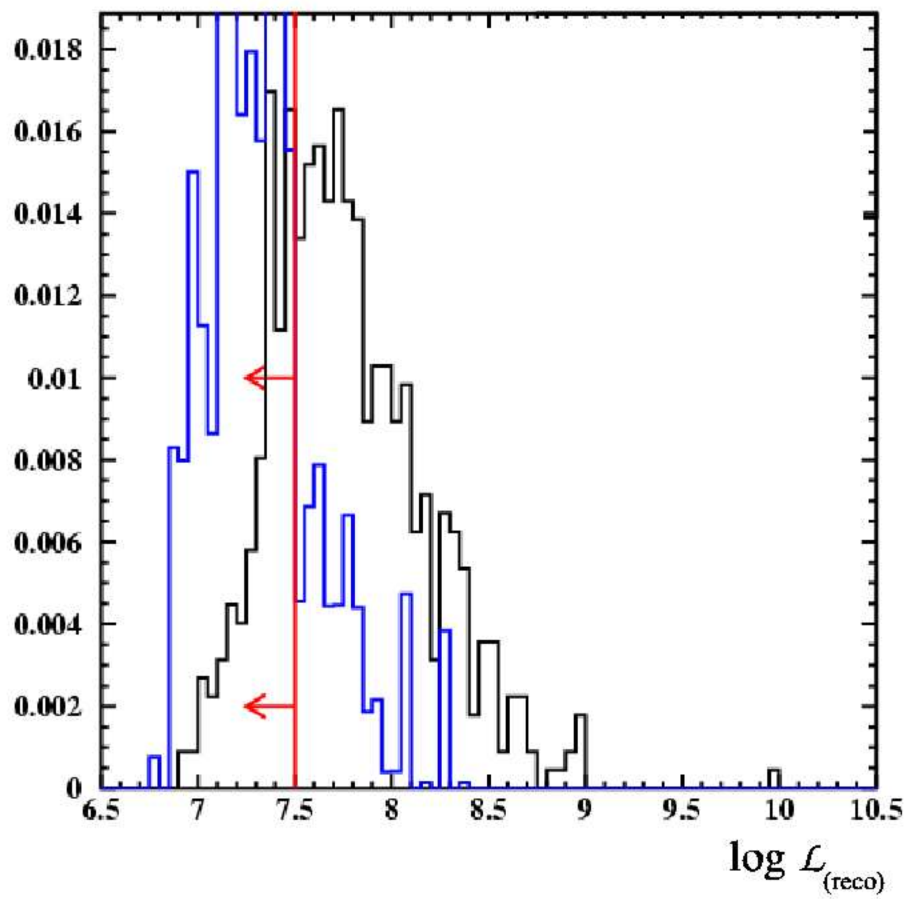

Figure 3.13: Likelihood of track reconstruction for a representative burst from the 2000 analysis with n-2 cuts applied (the spaceangle cut is not applied in order to maintain sufficient statistics). Simulated signal events are blue, observed background events are black, and the applied selection criterion is represented by a vertical red line.

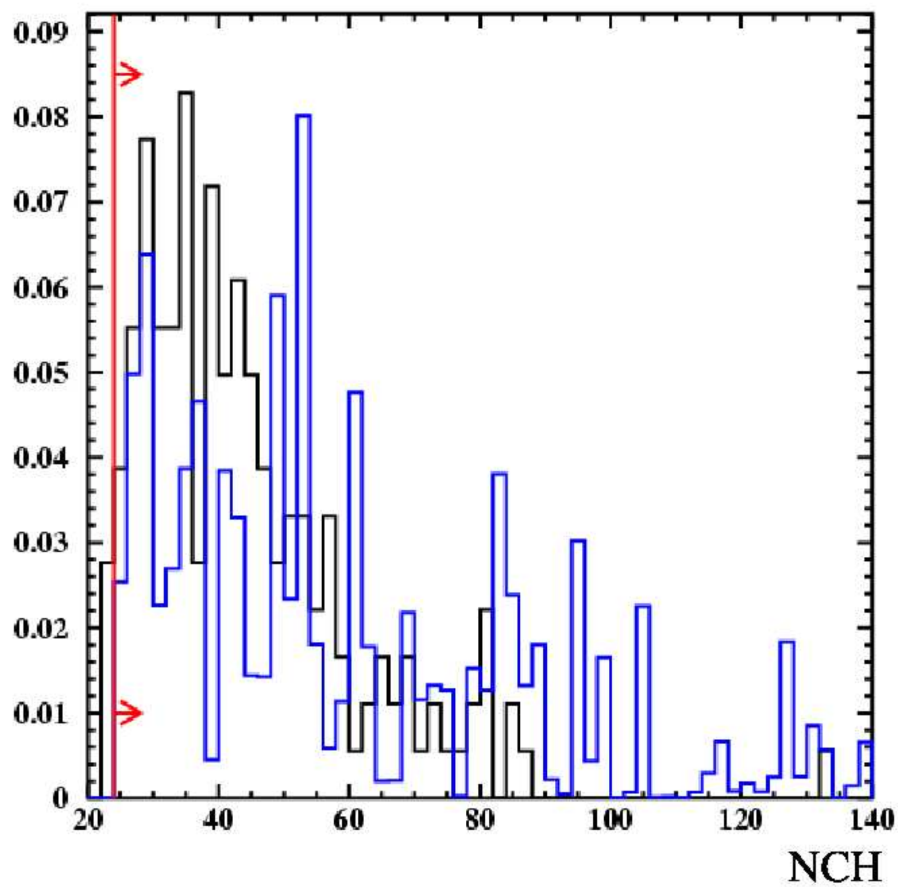

Figure 3.14: Number of Hit Channels (NCH) distribution for a representative burst from the 2000 analysis with n-2 cuts applied. Simulated signal events are blue, observed background events are black, and the applied selection criterion is represented by a vertical red line.

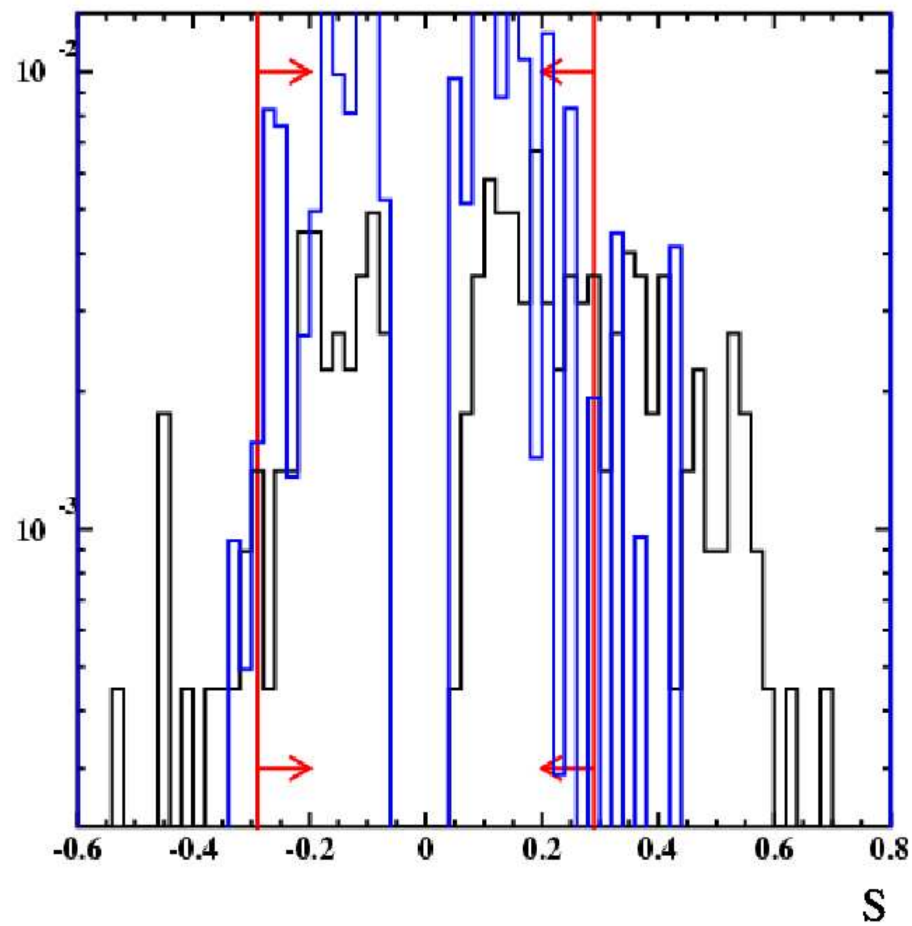

Figure 3.15: Smoothness distribution for a representative burst from the year 2000 analysis with n-2 cuts applied. Simulated signal events are blue, observed background events are black, and the applied selection criterion is represented by vertical red lines.

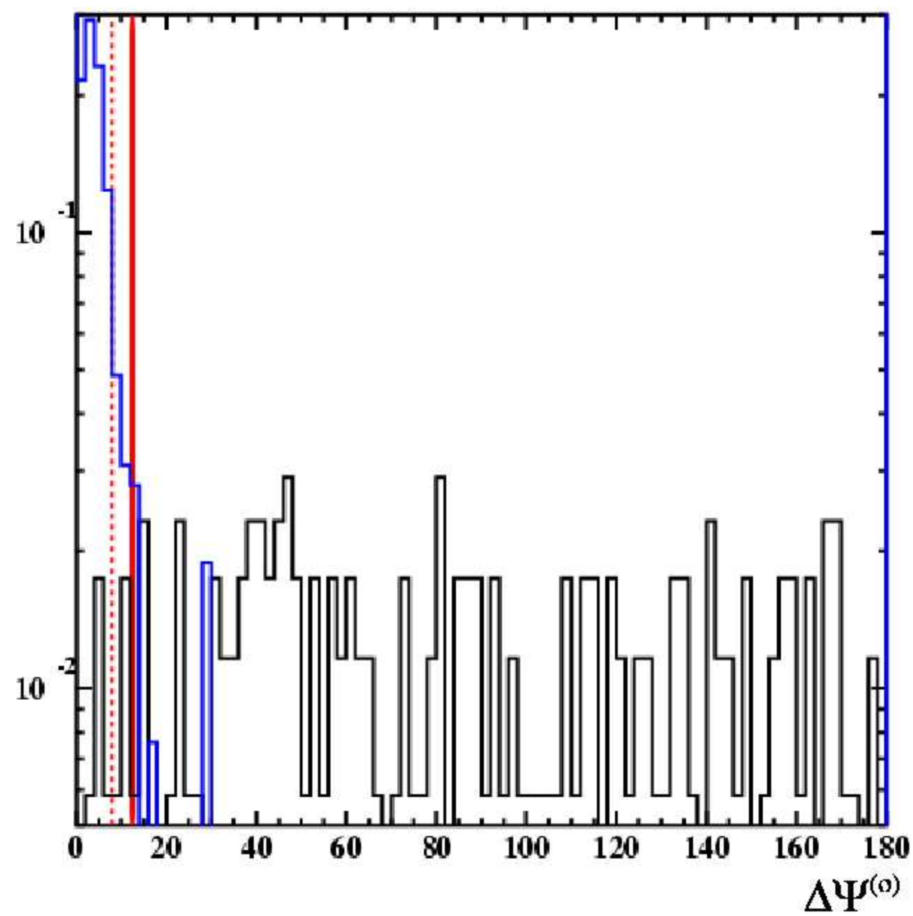

Figure 3.16: Spaceangle fit for a representative burst from the 2000 analysis with n-1 cuts applied. Simulated signal events are blue, observed background events are black, and the applied selection criteria are represented by vertical red lines for high-latitude (solid) and low-latitude (dashed) bursts.

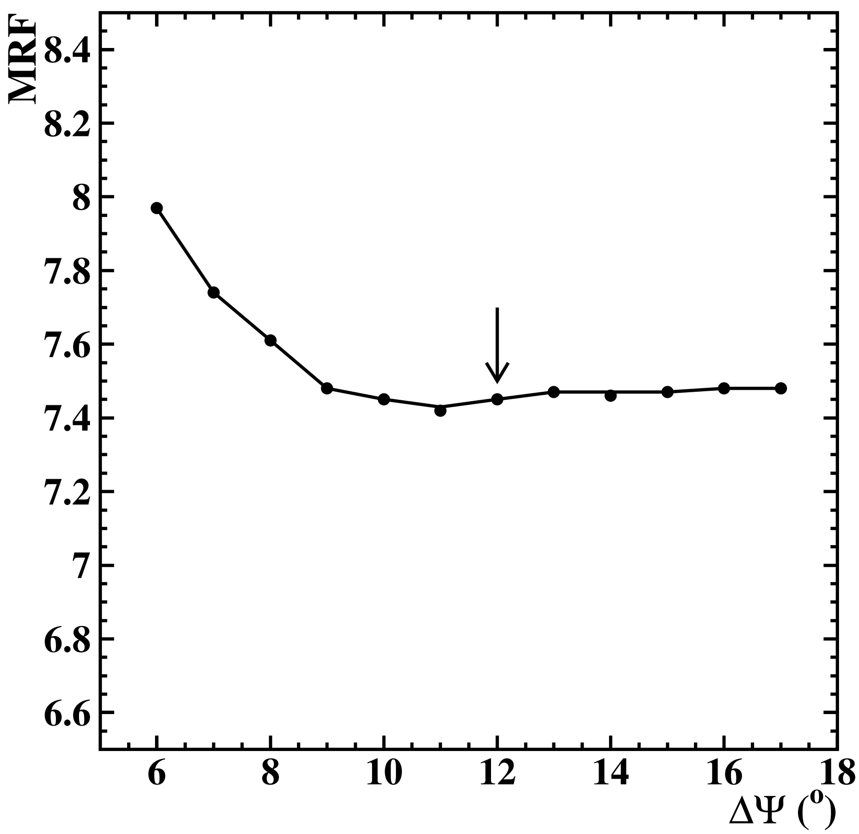

Figure 3.17: Relative Model Rejection Factor (MRF) as a function of angular mismatch ($\Delta\Psi_1$) between the burst position and the reconstructed track, for the subset of bursts from 2000. The arrow indicates the mismatch angle selected for this analysis.

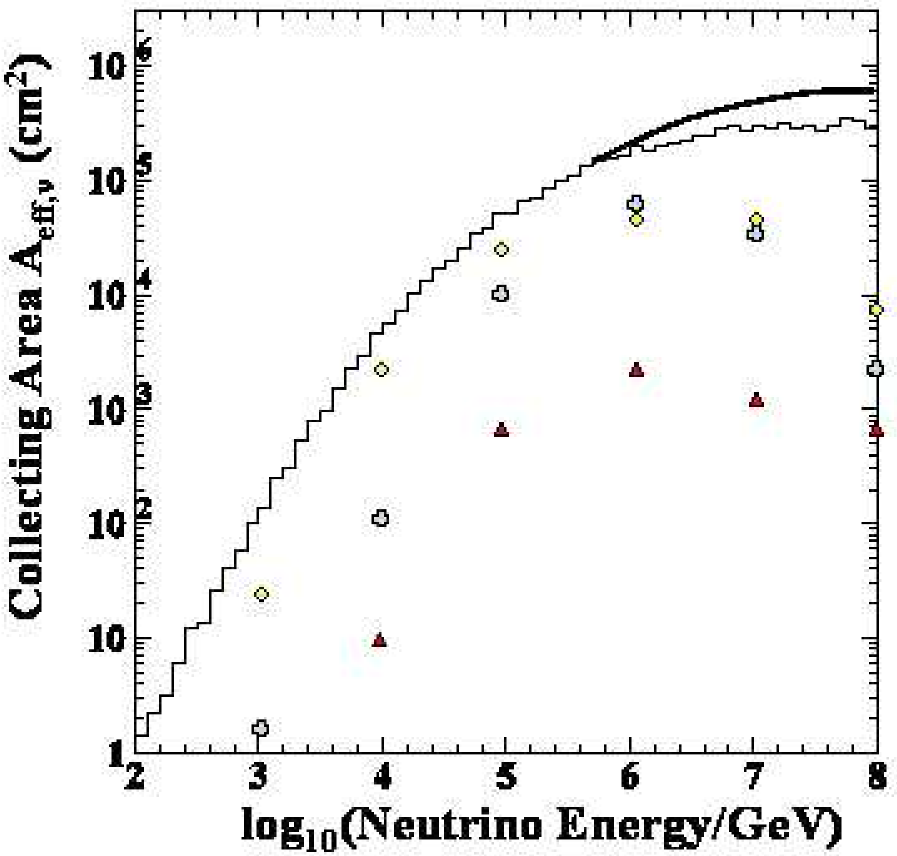

Figure 3.18: Angle-averaged muon neutrino effective area for the 2001-2003 AMANDA-II coincident search algorithm, based upon Monte Carlo simulations of expected signal events from the northern hemisphere. Also shown is the effective area without earth attenuation effects. Other AMANDA effective areas shown include the B-10 GRB analysis (blue crosses), the AMANDA-II Point Source analysis at zenith angle 50° (yellow diamonds), and the AMANDA-II Diffuse Analysis (red triangles). Minimally restrictive data selection criteria allow the GRB search to have the largest effective area of any AMANDA analysis.

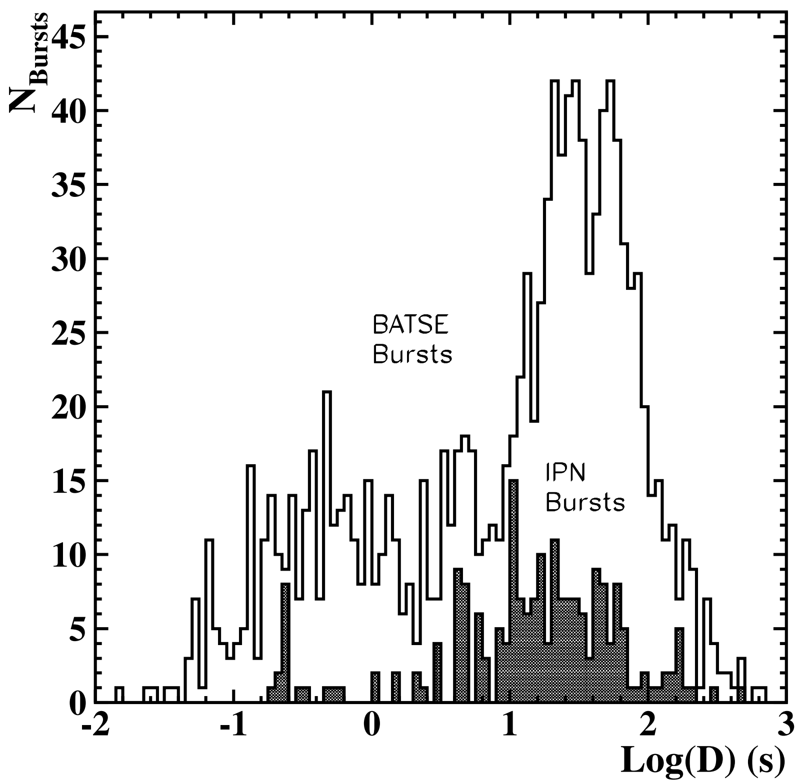

Figure 3.19: Duration distribution of BATSE GRBs (upper histogram) and IPN bursts for which durations have been determined (lower histogram). Both distributions appear to be drawn from the same underlying population.

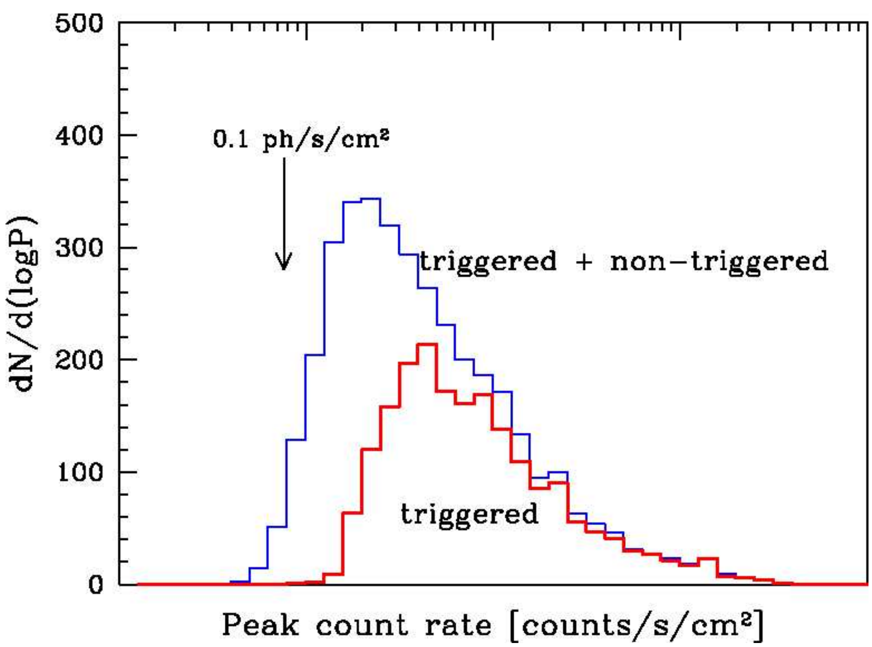

Figure 3.20: Peak Count Rate for BATSE triggered bursts (red histogram) and for triggered and non-triggered bursts together (blue histogram). The peak rate for triggered bursts is more than an order of magnitude higher than for non–triggered bursts.

Table 3.1: Primary Instruments in the Third Interplanetary Network

Instrument	Energy Range (keV)	Mission Homepage
BATSE LAD	30 - 190	http://www.batse.msfc.nasa.gov
BeppoSAX GRBM	40 - 700	http://www.asdc.asi.it/bepposax
BeppoSAX WFC	2 - 26	http://www.asdc.asi.it/bepposax
HETE-II FREGATE	6 - 400	http://space.mit.edu/HETE/fregate.html
HETE-II WXM	2 - 25	http://space.mit.edu/HETE/wxm.html
HETE-II SXC	2 - 14	http://space.mit.edu/HETE/sxc.html
INTEGRAL	15 - 10000	http://integral.esac.int/
Konus WIND	12 - 10000	http://www-spof.gsfc.nasa.gov/istp/wind/
Mars Odyssey	~100 - 8000	http://mars.jpl.nasa.gov/odyssey/
NEAR XGRS	100 - 1000	http://near.jhuapl.edu
RHESSI	~25 - ~25000	http://hesperia.gsfc.nasa.gov/hessi
Ulysses	25 - 150	http://ulysses.jpl.nasa.gov

Table 3.2: BATSE Triggered and IPN Bursts Per Year in the AMANDA Analysis, by Duration

Year	1997	1998	1999	2000	2001	2002	2003
N_{Short}	12	15	9	7	1	1	2
N_{Long}	51	50	61	77	15	21	24
$N_{Unknown}$	15	29	26	3	0	0	0
N_{Total}	78	94	96	87	16	22	26

Table 3.3: List of GRBs in the 2000-2003 Analysis

GRB ID	Alternate GRB ID	On–Time Duration	RA	DEC	BATSE Error Radius	Stern 1σ Error Radius	Comments
7988	11587d	1.947	136.77	4.80	3.25	4.5	Short Burst
N/A	11591c	8.	91.7	3.4	N/A	11.6	
7989	11591d	33.728	16.56	36.51	1.37	2.0	
7991	11593?	56	274.16	84.14	1.37	?	No T_{90}, Assigned Mean Duration
7992	11594a	5.158	182.04	65.95	4.23	4.5	
7994	11595b	27.779	125.76	77.70	0.45	0.0	
7995	11596b	2.531	53.99	60.60	5.60	11.1	Short Burst
N/A	11597b	74	317.3	55.4	N/A	12.3	
7997	11599a	21.918	110.56	0.53	2.35	1.8	
N/A	11599b	27.	113.3	17.3	N/A	7.4	
7998	11600a	11.948	143.68	29.82	1.64	1.8	

GRB ID	Alternate GRB ID	On–Time Duration	RA	DEC	BATSE Error Radius	Stern 1σ Error Radius	Comments
N/A	11600b	39.	245.6	50.7	N/A	9.3	
7999	11600?	1.696	330.03	16.89	12.39	?	Short Burst
8002	11602a	168.	236.52	65.16	3.90	3.1	
N/A	11602b	16.	206.4	20.6	N/A	6.8	
8004	11603a	68.	296.73	47.87	1.44	1.8	
8005	11604a	23.	3.69	72.68	1.00	1.2	
8008	11605b	25.197	58.20	54.28	0.53	3.7	
8009	11605f	27.073	174.46	30.66	3.40	2.8	
8012	11606b	23.184	275.83	62.05	2.52	2.3	
N/A	11608a	8.	159.9	48.0	N/A	8.8	
8019	11609e	63.92	226.07	40.92	1.46	1.4	
8022	11610d	24.636	88.49	6.80	0.53	0.6	
8030	11615a	25.454	320.29	37.92	0.72	0.8	
8031	11615e	28.	96.21	11.04	1.75	1.7	
8035	11616c	2.546	197.89	10.25	7.58	6.3	Short Burst

GRB ID	Alternate GRB ID	On–Time Duration	RA	DEC	BATSE Error Radius	Stern 1σ Error Radius	Comments
8036	11617b	189.365	137.71	50.66	1.72	2.2	
8039	11620e	98.902	27.22	32.66	2.79	6.3	
8045	11623a	65.616	82.48	4.44	2.39	2.9	
8047	11624c	2.009	49.24	36.39	4.09	3.9	Short Burst
N/A	11625b	44.	170.3	59.0	N/A	15.7	
8049	11626a	78.515	190.73	48.08	0.98	0.0	
N/A	11633b	44.	155.5	50.6	N/A	9.8	
8057	11633?	56.	358.31	39.26	4.79	?	No T_{90}, Duration Assigned
N/A	11633f	137.	308.0	3.1	N/A	3.8	
N/A	11634g	18.	135.2	47.7	N/A	17.6	
8061	11634j	30.169	32.00	59.77	3.72	3.5	
8063	11636b	11.849	343.53	6.65	0.79	1.2	
N/A	11637c	41.	146.8	28.1	N/A	8.3	
8064	11637d	158.772	57.20	24.69	3.54	1.5	

GRB ID	Alternate GRB ID	On–Time Duration	RA	DEC	BATSE Error Radius	Stern 1σ Error Radius	Comments
N/A	11637e	62.	322.9	9.7	N/A	15.8	
N/A	11638b	152.	129.1	27.4	N/A	2.6	
8069	11642a	6.12	138.51	67.22	1.43	0.0	
N/A	11642d	7.	180.0	50.7	N/A	12.4	
8071	11643b	46.762	264.37	80.82	5.10	4.8	
N/A	11644b	28.	101.3	15.0	N/A	3.2	
N/A	11644f	6.	212.9	16.6	N/A	5.0	
N/A	11646c	9.	53.1	4.9	N/A	8.7	
8074	11649?	56.	175.47	68.27	8.72	?	No T_{90}, Assigned Mean Duration
8075	11649c	22.956	134.85	69.42	0.81	0.4	
N/A	11650a	55.	277.3	26.2	N/A	3.3	
8077	11651d	4.845	222.39	2.93	5.06	8.9	Short Burst
8079	11652e	5.80	69.80	76.15	5.37	5.8	

GRB ID	Alternate GRB ID	On–Time Duration	RA	DEC	BATSE Error Radius	Stern 1σ Error Radius	Comments
N/A	11652g	42.	64.5	33.7	N/A	3.5	
N/A	11654b	93.	104.1	54.2	N/A	0.9	
8084	11655b	86.830	174.91	16.98	3.09	0.4	
8085	11658b	4.912	223.06	71.80	1.38	1.3	
8086	11658c	22.2185	105.03	53.98	0.95	7.2	
N/A	11663b	56.	358.6	19.4	N/A	10.8	
N/A	11663f	47.	8.2	4.7	N/A	6.1	
N/A	11668c	46.	38.1	18.1	N/A	7.5	
8097	11672a	2.994	202.72	3.78	7.54	7.8	Short Burst
8099	11672f	17.064	89.89	2.39	0.55	1.1	
N/A	11672h	147.	83.3	25.3	N/A	2.3	
N/A	11675e	98.	48.7	38.0	N/A	1.6	
8109	11681b	11.00	107.98	76.74	1.05	1.3	
8111	11683a	17.258	346.03	3.33	1.03	0.9	
010213	010213	45335.	30	10:31:36	+05:30:39	$r = 30'$	

GRB ID	Alternate GRB ID	On–Time Duration	RA	DEC	BATSE Error Radius	Stern 1σ Error Radius	Comments
010214	N/A	31687.	18.	17:40:46	+48:33:50	r = 3′	
010220	N/A	82267.	150	02:36:59	+61:45:58	r = 4′	
010222	N/A	26610.	80.	14:52:16	+43:02:06	r = 2.5′	
010324	N/A	41558.	375.	07:11:10	+20:05:20	3′ x 13′	
010412	N/A	78360.	80.	19:39:34	+13:37:12	r = 6′	
010607	N/A	53722	50	16:21:??	+18:12:??	1.6° x 4.0°	
010613	1547	27233.	150	17:01:??	+14:18:??	1000 sq. arcmin.	
010628	N/A	4203.3	1.	01:12:??	+13:01:??	2′ x 1.5′	
010706	N/A	29946.	60.	17:18:??	+27:42:??	0.9° x 1°	
010721	N/A	14203.	4.	04:11:??	+12:21:??	30′ x 30′	
010726	N/A	05483.	6.	02:01:??	+05:40:??	23′ x 4′	
010801	N/A	72800.	16.	00:13:??	+14:14:??	6′ x 14′	
010802	N/A	30922.	5.	12:34:56	+04:52:48	18′ x 40′	

GRB ID	Alternate GRB ID	On–Time Duration	RA	DEC	BATSE Error Radius	Stern 1σ Error Radius	Comments
010921	1761	18950.6	25.	22:54:23	+40:54:??	250 sq. arcmin.	
010928	1770	60826.6	40	23:28:??	+30:41:??	10 deg x 4′	
011008	N/A	71752	15	20:13:??	39:59:??	8.5° x 5°	
020214	N/A	67776.	20	14:24:??	+31:48:??	1′ x 2.4′	
020221	N/A	29264.	20.	03:15:??	+36:16:??	1.2′ x 3′	
020311	N/A	04892.	13.	04:28:??	+61:11:??	1.5′ x 2.5′	
020317	1959	65731.	10.	10:21:21	+12:44:38	r = 18′	
020409	N/A	76285.	59.1	08:45:14	+66:41:16	3.2 arcmin	
020625	2081	41149.3	125.	20:44:14	+07:10:12	18′ x 32′	
020708	N/A	16451.	150.	07:58:05	+41:35:39	110 sq. arcmin.	
020714	N/A	56970.	20.	12:09:04	+83:06:44	200 sq. arcmin.	GCN1457

GRB ID	Alternate GRB ID	On–Time Duration	RA	DEC	BATSE Error Radius	Stern 1σ Error Radius	Comments
020715	N/A	69663.	<10.	13:50:13	+61:50:44	140 sq. arcmin.	GCN1454
020819	2275	53855.	20.	23:27:14	+06:17:56	r = 130″	
020923	N/A	47182	5.	14:06:08	+50:31:18	11.6 arcmin	1st of 2 error boxes
020923	N/A	47182.	5.	9:20:15	+59:56:35	11.6 arcmin	2nd of 2 error boxes
021004	H2380	43573.6	100.	00:26:57	+18:55:44	arcsec. (Afterglow Observed)	
021016	2397	37740.	50.	00:33:44	+46:47:16	200 sq. arcmin.	
021020	2413	72772.	20.	21:29:11	51:55:00	20 sq. arcmin.	
021104	H2434	25262.9	29.6	03:53:??	37:57:??	24′ x 42′	

GRB ID	Alternate GRB ID	On–Time Duration	RA	DEC	BATSE Error Radius	Stern 1σ Error Radius	Comments
021112	H2448	12495.9	>5.	02:36:52	+48:50:56	r = 20′	
021113	2449	23936.9	20	01:33:53	+40:27:45	r = 2′ x 9′	
021211	2493	40714.	>5.7	08:09:04	+06:43:33	arcsec. (Afterglow Observed)	
030226	U10893	13592.0	>100.	11:33:05	+25:53:53	arcsec. (Afterglow Observed)	
030227		31320.	20.	04:57:29	+20:29:23	r = 5′	Timing Uncertainty of Order 1 min.
030324	2641	11562.	12.	13:37:11	-00:19:22	.6″ (Afterglow Observed)	

GRB ID	Alternate GRB ID	On–Time Duration	RA	DEC	BATSE Error Radius	Stern 1σ Error Radius	Comments
030329	2652	41834.7	>25.	10:44:50	+21:31:23	arcsec (Afterglow Observed)	
030331	N/A	20320.8	25.	23:17:02	+36:15:36	400 sq. arcmin.	
030413		27277.	15.	13:14:25	+62:20:55	314 sq. arcmin.	
030422	N/A	28275.	10.	19:05:34	+13:47:00	24000 sq. arcmin.	2 error boxes, 1 So. Hem
030425	N/A	56911.	500.	15:33:11	+26:17:30	2300 sq. arcmin.	
030501B	N/A	04637.	8.	18:54:19	+23:52:30	400 sq. arcmin.	
030509	N/A	21024.	9.	05:26:24	+07:08:48	124 sq. arcmin.	

GRB ID	Alternate GRB ID	On–Time Duration	RA	DEC	BATSE Error Radius	Stern 1σ Error Radius	Comments
030626	N/A	06354.	40.	19:03:36	+03:49:35	9900 sq. arcmin.	
030706	N/A	00135.	10.	09:46:46	+01:49:41	1200 sq. arcmin.	
030714	N/A	80086.	6.	15:06:22	+19:58:02	10000 sq. arcmin.	
030817	2808	01467.7	50. (assumed)	19:15:47	+10:48:30	r = 1 deg	Duration likely < 57 sec. Located near x-ray source
030823	2818	31690.6	78.4 (T_{90})	21:30:47	+21:59:46	12′ x 5′	XRF
030824	2821	60455.1	>16. (T_{90})	00:05:02	+19:55:37	r = 11.2′	XRF
030827	N/A	58120.	5.	14:52:46	+48:35:40	25000 sq. arcmin.	
030913	2849	61617.5	7.9	20:58:02	-02:12:32	r = 30′	close to horizon

GRB ID	Alternate GRB ID	On–Time Duration	RA	DEC	BATSE Error Radius	Stern 1σ Error Radius	Comments
030921	N/A	31103.	16.	22:27:14	+05:44:21	1100 sq. arcmin.	
030922	N/A	31404.	35.	15:18:18	+25:30:07	30000 sq. arcmin.	
030926		60748.	0.18	11:29:28	+42:54:05	6700 sq. arcmin.	
031026	2882	20143.2	114.2 (T_{90})	03:18:42	+28:21:58	r = 15′	
031026B	N/A	05188.	0.2	22:24:00	+0:06:51	4500 sq. arcmin.	
031111A	2924	60313.	10.	71:45:??	+18:06:??	24 sq. arcmin.	
031111B	2925	71487.	35.4	03:59:20	+34:36:57	r = 30′	XRF?
031220	2976	12596.7	23.7	04:51:17	+27:20:47	> .3° x 1°	

Table 3.4: Data Selection Criteria, Year by Year

Criterion	97-99	00	01-03	Precursor[a]
$\Delta\Psi_1$, $\delta \geq 10°$ ($\delta < 10°$)	<20° (<6.5°)	<12.5° (<7°)	<12° (<8°)	<12° (<5°)
$\Delta\Psi_2$, $\delta \geq 10°$ ($\delta < 10°$)	N/A	N/A	<12° (<8°)	<12° (<6°)
$\Delta\Psi_3$, $\delta \geq 10°$ ($\delta < 10°$)	N/A	N/A	<16° (<8°)	<16° (<8°)
$\Delta\Psi_4$, $\delta \geq 10°$ ($\delta < 10°$)	N/A	N/A	N/A	<40° (<40°)
σ_Ψ[b]	N/A	N/A	<5° (<5°)	<5° (<5°)
Track Uniformity	N/A	<0.29 (<0.29)	<0.55 (<0.55)	<0.55 (<0.55)
$£_{reco}$[c]	N/A	<7.85 (<7.5)	N/A	N/A
Direct Hits	>10	N/A	N/A	N/A
N_{OMs} in Event	N/A	N/A (>24)	N/A	N/A
Signal Passing Rate	0.35 (0.22)	0.69 (0.54)	0.68 (0.61)	0.69
$N_{\mathrm{Sig,WB}}$[d]	0.30	0.27	0.21	N/A
$N_{\mathrm{Sig,MN}}$[e]	0.40	0.48	0.37	N/A
$N_{\mathrm{Sig,Razz}}$[f]	0.82	1.0	0.77	N/A
$N_{\mathrm{Sig,Pre}}$[g]	N/A	N/A	N/A	0.16

[a]The precursor time period was searched only during the 2001-2003 dataset.
[b]The angular resolution of the paraboloid fit.
[c]The log(Likelihood) of the reconstructed track.
[d]Based on the flux of Waxman (2003), corrected for neutrino oscillations.
[e]Based on the flux of Murase & Nagataki (2006a).
[f]Based on the "supranova" flux of Razzaque et al. (2003a).
[g]based on the "precursor" flux of Razzaque et al. (2003b).

Table 3.5: Systematic Uncertainties/Corrections in the GRB Analysis

Source of Uncertainty	Quantity	Reference
OM sensitivity	±7%	Ahrens et al. (2004)
Simulation parameters (including ice properties)	±15%	Sections 3.3 & 3.4
Neutrino-nucleon cross-section	±3%	Gandhi et al. (1998)
Uncertainties added in quadrature	+17/-17%	
Correction for IPN bursts not included in models	-3%	Appendix A
Correction for short bursts inappropriately included in models	-6%	Appendix A
Total	+8%/-26%	

Chapter 4

Results

We observe zero events from the 419 Northern Hemisphere bursts searched during the years 1997 to 2003, which is consistent with the expected number of background events (Table 4.1). We then determine the Model Rejection Factor according to Equation 3.1 based upon the observed and expected background events (Table 4.1) and expected signal events (Table 3.4). The MRF for the 2000-2003 analysis applied to a Waxman-Bahcall spectrum is 2.5; thus the muon neutrino flux upper limits have at normalization at 1 PeV of

$E^2\Phi_\nu \leq 1.1 \times 10^{-8}$ GeVcm^{-2}s^{-1}sr^{-1},

with 90% of the events expected between ∼10 TeV and ∼3 PeV.

Since the observed number of events is less than the expected background, the flux upper limits for the combined 7–year coincident muon neutrino search are approximately a factor of three better than the expected sensitivity (i.e. the observed MRF for a Waxman-Bahcall flux is 1.3 compared to the expected value of 3.8). Figure 4.1 shows the 90% C.L. flux upper limits for the combined 7–year analysis relative to the Waxman-Bahcall, Razzaque, and Murase-Nagataki models. Though our analysis was restricted to bursts located in the Northern Hemisphere (2π sr), all flux upper limits are for the entire sky (4π sr). Including the systematic uncertainties in the manner outlined by Conrad et al. (2003), we calculate the coincident muon neutrino flux upper limit for the Waxman-Bahcall spectrum to have a normalization at 1 PeV of

$E^2\Phi_\nu \leq 6.0 \times 10^{-9}$ GeVcm^{-2}s^{-1}sr^{-1},

with 90% of the events expected between ∼10 TeV and ∼3 PeV.

We place similar constraints on the model parameters of Murase & Nagataki

(2006a). Based on our null result, Parameter Set C is highly disfavored for all variations in their parameters, though this particular set is disfavored on other grounds as well, and is only briefly described in their work. Parameter Set A is ruled out (MRF=0.82) by the current AMANDA observations at the 90% confidence level. However, it is important to note that Parameter Set A uses a baryon loading factor that is fine-tuned to provide significant neutrino flux. Other, possibly more realistic, values for the baryon loading would significantly reduce the expected neutrino emission, and therefore result in an MRF that is higher by an order of magnitude or more. The original model incorporates only long-duration bursts that follow the cosmic star-formation rate (Murase & Nagataki , 2006c); incorporating all short bursts would yield flux upper limits that are better than those presented here by approximately 13%, which includes removing the "correction" due to incorporating of bursts of unknown duration (see Section 3.4).

Our combined results from 1997-2003 also constrain the supranova model of Razzaque et al. We begin by considering the assumption that all GRBs are preceded by supernovae that produce a circumburst environment ideally suited for neutrino production. The observed MRF for this case is 0.40, and thus we exclude the predicted neutrino flux at the 90% level. Furthermore, the flux upper limit determined for this model is derived from observations of long bursts only. As with the results of Murase & Nagataki (2006a), if this model is expanded to include short-duration bursts, the flux upper limit improves by approximately 13%. However, only a very small number of all bursts (~4 out of many thousands) have been observed in association with SNe. And, as described in Chapter 2, at least a fraction of these SNe did not occur at an ideal time relative to the burst. Thus, AMANDA's results confirm previous observations that lead us to expect less than maximal emission from this model of GRB neutrino production.

Comparison of our observations with the predictions of the Cannonball model require a different treatment than the other models. As described in Chapter 2 (and in Dar & DeRújula (2001)), the Cannonball model predicts an observed flux of several neutrinos per burst, but only for the 10% of bursts that are classified within the highest decade of observed photon flux ($F_{BATSE} > 10^{-5}$ erg cm^{-2}. Furthermore, because the neutrino beam is predicted to be narrower than the photon beam (with a solid angle smaller by a factor of ~100), neutrinos will only be seen for bursts that are viewed very close to the axis of the jetted emission. Together, the factor of 1/10 and 1/100 lead us to expect one significant neutrino source per 1000 bursts. Because we have searched for neutrino emission from 419 bursts, we cannot yet constrain the Cannonball model. We can, however, state that if this model is correct, then the solid angle of the neutrino jet must be smaller than that of the photon jet by approximately a factor of 40 or more.

Finally, we observe zero events (on an expected background of 0.2 events) from the precursor time period of the bursts from 2001-2003 (Table 4.2). The precursor model of neutrino production was tested for only a small subset of the long-duration bursts, and the neutrino energy spectrum peaks at a level where the AMANDA-II sensitivity is greatly reduced. Thus, the flux upper limit for the precursor model is significantly less restrictive (MRF = 14). As described in Chapter 3, We also searched for neutrino emission from 153 additional non-triggered bursts discovered in the BATSE archival data; we observed zero events from these bursts as well. Because most theoretical models were based upon BATSE triggered bursts only, we do not include the results from the non-triggered burst search in the flux upper limits or MRF determinations. If models are constructed in the future which explicitly take into account these bursts, then any comparison with these observations must also account for the significantly lower expected flux of neutrinos from each burst ($F_{non} \sim F_{trig}/20$ on average, assuming $E_\nu \propto E_\gamma$).

The results of these analyses can also be applied to any other hypothesized spectrum by using the Green's Function Fluence Limit formula, in a method similar to that presented by the Super-Kamiokande Collaboration (Fukuda et al. , 2002). By folding the energy-dependent sensitivity of the detector into a desired theoretical spectrum, one can straightforwardly calculate a flux upper limit for that specific spectrum. The Green's Function fluence upper limit for AMANDA-II (Figure 4.2) extends several orders of magnitude in energy beyond the range of the Super-Kamiokande limit, and is approximately an order of magnitude lower than the Super-Kamiokande results in the region of overlap, primarily due to the much larger effective area of AMANDA-II. For example, at 100 TeV we calculate $F_\nu \leq 1.7 \times 10^{-7}$ cm^{-2} (see also Appendix B). As this method does not rely on averaging burst properties (as many specific models do), it is particularly effective for incorporating large burst-to-burst variations in expected muon neutrino flux (e.g. for GRB030329, see Stamatikos , 2006).

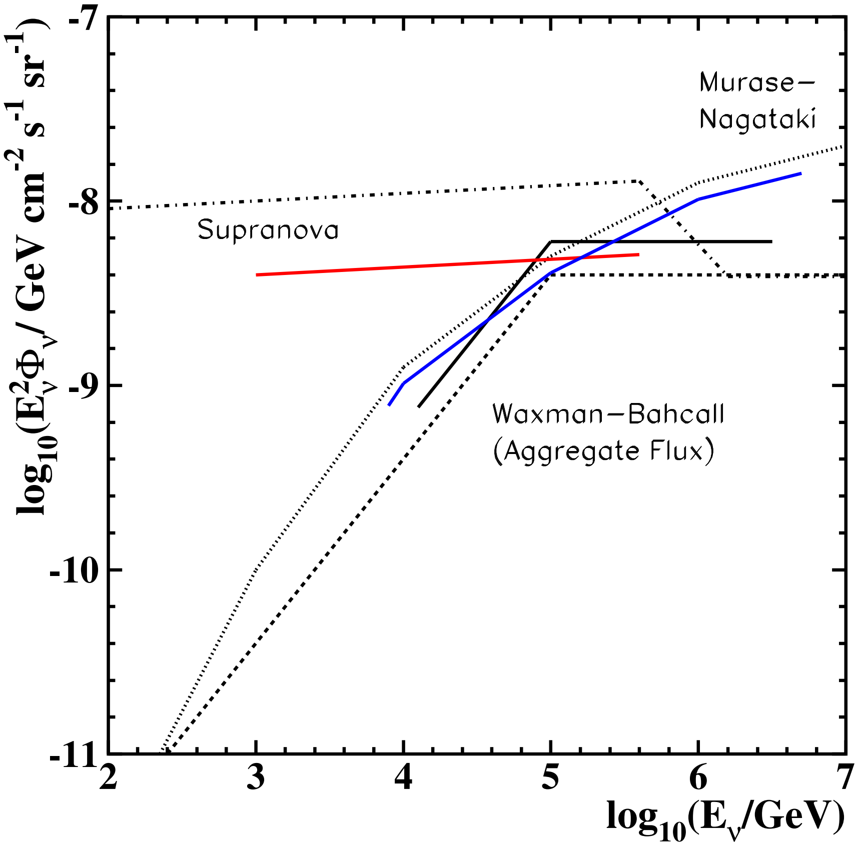

Figure 4.1: AMANDA flux upper limits (solid lines) for muon neutrino energy spectra predicted by the Waxman-Bahcall spectrum (Waxman , 2003) (thick dashed line), the supranova spectrum (Razzaque et al. , 2003a) (dot-dashed line) and the Murase-Nagataki spectrum (Murase & Nagataki , 2006a) (thin dotted line). The central 90% of the expected flux for each model is shown. For the Waxman-Bahcall model we include both long- and short-duration bursts; for the other spectra, only long-duration bursts are included. Including short-duration bursts would improve the flux upper limits by approximately 13%. While our analysis was restricted to bursts located in the Northern Hemisphere (2π sr), all flux upper limits are for the entire sky (4π sr).

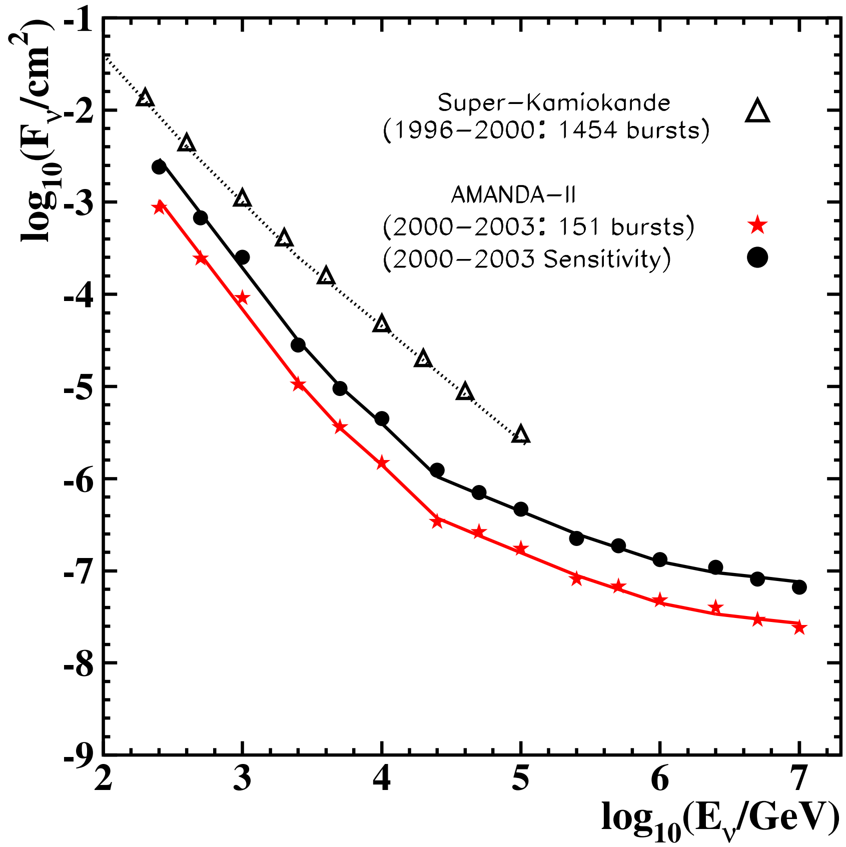

Figure 4.2: Green's Function Fluence Upper Limit for AMANDA's GRB analysis from 2000 to 2003. This fluence upper limit can be folded into any desired spectrum to provide a flux upper limit for that particular spectrum.

Table 4.1: Results of the Coincident GRB Analysis 1997-2003

Year	1997-1999	2000	2001-2003	2000-2003	1997-2003
N_{Bursts}	268	87	64	151	419
$N_{\mathrm{BG,Exp}}$	0.46	1.02	0.27	1.29	1.74
N_{Obs}	0	0	0	0	0
Event Upper Limit	1.98	1.50	2.30	1.30	1.10
$MRF_{\mathrm{WB}}{}^{a}$	6.6	5.5	11	2.5	1.3
$MRF_{\mathrm{MN}}{}^{b}$	4.9	3.1	6.2	1.4	0.82
$MRF_{\mathrm{Razz}}{}^{c}$	2.4	1.5	3.0	0.68	0.40

[a] Based on the flux of Waxman (2003), corrected for neutrino oscillations.
[b] Based on the flux of Murase & Nagataki (2006a).
[c] Based on the "supranova" flux of Razzaque et al. (2003a).

Table 4.2: Results of Precursor Search 2001-2003

Year	N_{Bursts}	$N_{\text{BG,Exp}}$	N_{Obs}	Event U.L.	MRF
2001	15	0.06	0	2.38	
2002	21	0.07	0	2.37	
2003	24	0.07	0	2.37	
2001-2003	60	0.20	0	2.30	14

Chapter 5

Conclusion and Outlook

The AMANDA dataset has been searched for muon neutrino emission from more than 400 GRBs based on temporal and spatial coincidence with photon detections from numerous other observatories. We determined that the detector was operating in a stable fashion during all of these bursts, and we have shown that the application of a number of data selection criteria lead to an optimized value of the Model Rejection Factor for the Waxman-Bahcall neutrino spectrum. After the application of these criteria, zero neutrino events were observed in coincidence with the bursts, resulting in the most stringent upper limit on the muon neutrino flux from GRBs to date. We have compared this limit to the flux predictions from several prominent GRB models based on averaged burst properties. We constrain the parameter space of a number of these models at the 90% confidence level; in particular, our flux upper limit is more than a factor of 2 below the most optimistic predictions of Razzaque et al. However, we do not yet rule out the predictions of the canonical Waxman & Bahcall model, or alternate predictions such as the Cannonball model of Dar & DeRujula. Additionally, because individual bursts vary significantly in their expected neutrino spectra, we have presented a spectrum-independent method for determining flux upper limits for these bursts. The observations detailed in this work will play a significant role as future analyses seek to further constrain various theoretical models.

Finally, AMANDA's search for muon neutrinos from more recent GRBs will benefit greatly from the advanced capabilities of the Swift satellite (Burrows et al. , 2005), as will the GRB searches of other neutrino observatories currently in operation (Spiering et al. , 2004; Resvanis et al. , 2003; Aguilar et al. , 2006). While Swift's rate of GRB detections is lower than that of BATSE, the spatial localizations of the bursts by Swift are much more precise, which will obviate the need for a special analysis of poorly-localized bursts with its accompanying reduction in signal detection efficiency. Future missions, including the Gamma-Ray Large Area Space Telescope (Carson , 2006) will provide an even greater number of GRB localizations for use in neutrino searches. Furthermore, while analyses similar to the one presented here will continue to search specifically for muon neutrino flux in coincidence with photon observations of gamma-ray bursts, the method described here can be expanded to search for neutrinos correlated with other transient point sources as well (see Appendix C). In the future, AMANDA and its successor, IceCube, will have many more opportunities to detect neutrino emission from a host of astrophysical sources. Construction of IceCube is currently underway, and the instrumented volume for the partial detector is already significantly larger than the final instrumented volume of AMANDA. A diagram of the current and final states of the IceCube Observatory are shown in Figure 5.1, while Figure 5.2 provides a timeline for construction. The expected observational results of IceCube after three years of full detector operation are given in Figure 5.3. A fully-instrumented IceCube detector should surpass AMANDA's flux upper limits within its first few years of operation. However, it is important to note that the Observatory is operational even while under constrcution–in fact, IceCube is expected to have more than 1 km^3yr of integrated observations well before its targeted completion date. Coupled with the results presented here, IceCube will provide significant observations of astrophysical neutrino sources well into the future.

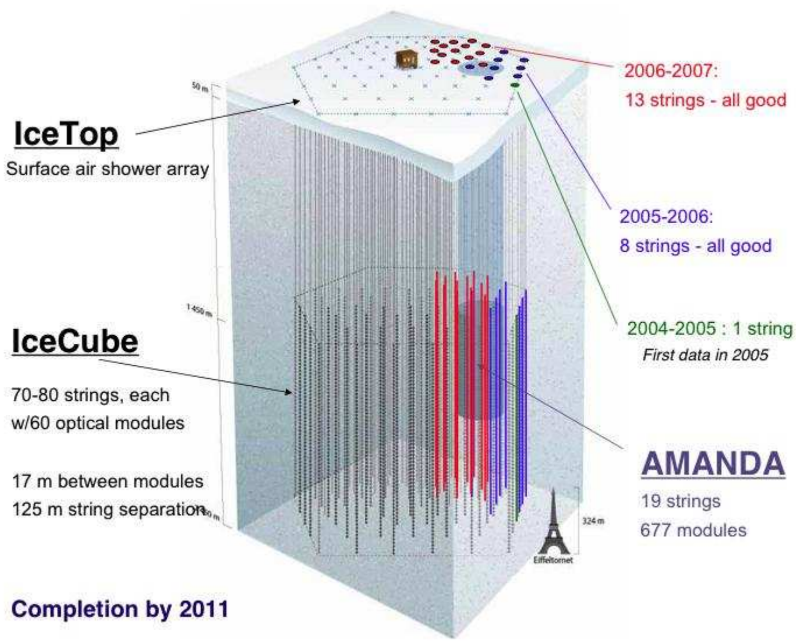

Figure 5.1: A diagram of IceCube showing the current status of the detector. The strings already installed are shown in green and red; AMANDA strings are shown in magenta.

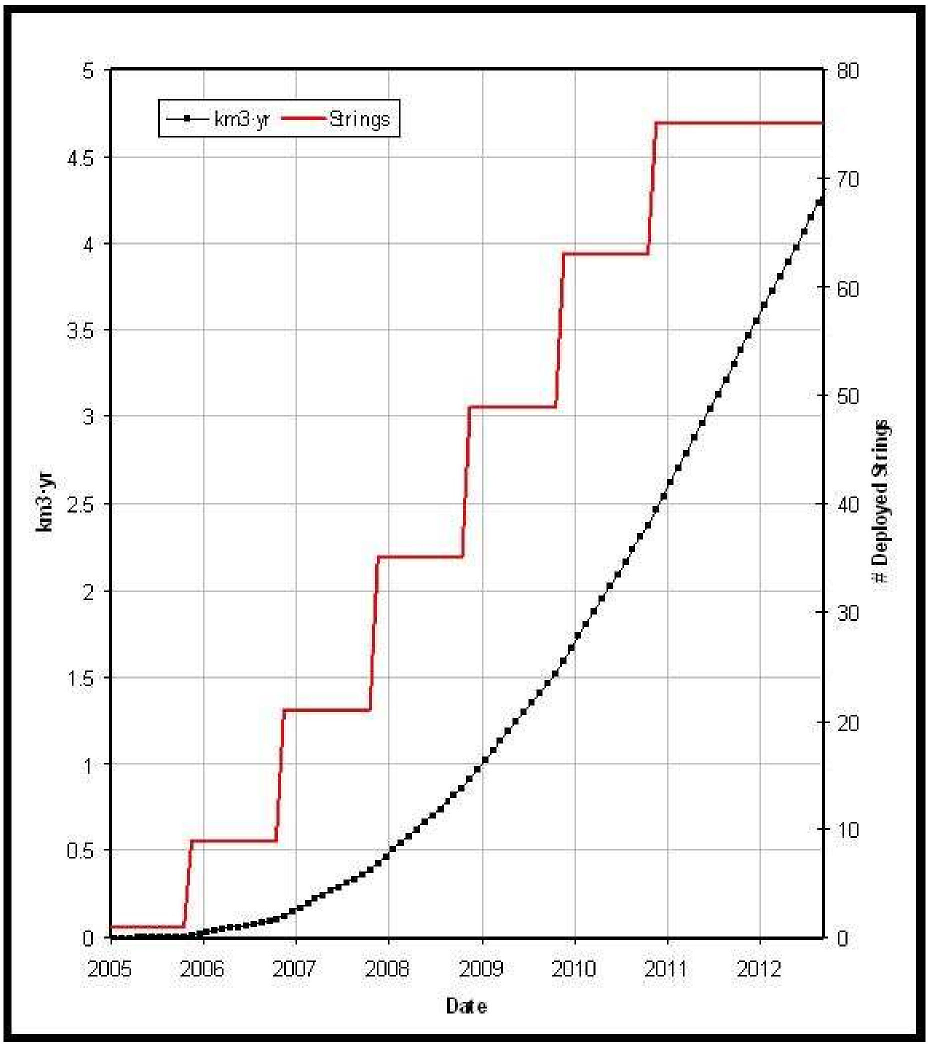

Figure 5.2: The number of installed strings and effective collecting area expected for IceCube during construction.

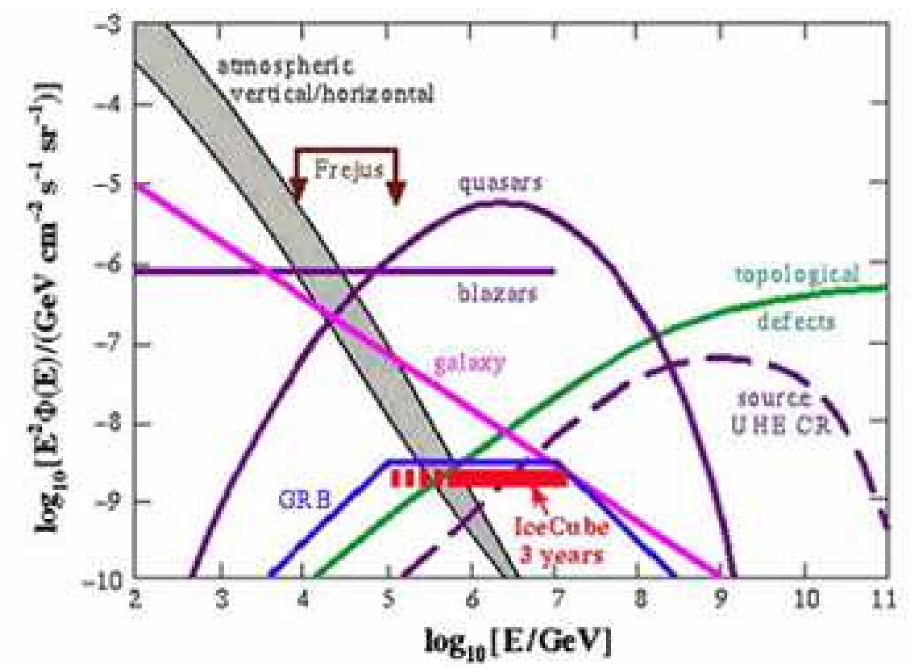

Figure 5.3: Flux Upper Limits for IceCube's 3-year diffuse analysis. Several prominent models for neutrino emission from various sources are also shown.

Appendices

A Model-Dependent Statistical Corrections to Flux Upper Limits

Though the ν flux formulation of Waxman (2003) explicitly links GRB neutrinos to the UHECR flux, elsewhere a formulation based on BATSE observations is treated in a comparable fashion, and is considered to arise from the same underlying phenomena (Waxman & Bahcall , 1997). Thus it is necessary to address the limitations introduced by AMANDA's reliance upon BATSE observations. As described in Section 3.4, models defined initially in terms of BATSE observations were also applied to bursts detected by the other IPN satellites. However, we cannot assume that characteristics of bursts detected by satellites with different sensitivities are completely identical. Since BATSE was decommissioned in May of 2000, there is no longer a way to cross-correlate the two datasets. Non-triggered BATSE bursts have on average less than 1/10 of the peak photon flux of the triggered bursts; assuming that the energy of neutrinos scales with the energy carried by gamma rays, we expect only a small fraction of the standard neutrino flux from these non-triggered bursts. Thus, if non-triggered bursts are inadvertently included in the flux upper limit, they will artificially improve that limit, because the extra bursts are assumed to have a larger neutrino flux than they would actually possess.

During the period of simultaneous operation from 1991 to 2000, 1088 IPN bursts were observed by BATSE, 953 of which were triggered. Undoubtedly some of these bursts did not trigger BATSE for reasons other than a lower flux. For example, BATSE may have been powered down, may have been in the vicinity of the South Atlantic Anomaly, or may have experienced unrelated on-board performance problems. However, we assume conservatively that all such bursts did in fact exhibit the lower flux common to non-triggered bursts. Therefore, ~12% of the IPN bursts should not actually be a part of the dataset that is compared with the models that are based upon BATSE's triggered GRB rate. Because IPN bursts are expected to contribute ~25% of our detectable signal, this effect reduces the total expected neutrino flux by ~3%. This correction is applied asymmetrically to the overall uncertainty, because it can hinder, but not improve, the effectiveness of the analysis (see Table 3.5).

For models based solely on long-duration bursts, such as Murase & Nagataki (2006a) and Razzaque et al. (2003a), the inclusion of bursts of unknown duration may also lead to an overestimation of the expected signal events, and thus a flux upper limit that is too restrictive. In order to ensure that we would not exclude potentially detectable neutrino events, the 75 bursts of unknown duration included in the dataset are assumed to last 100 s (for 1997-1999) or 50 s (for 2000-2003). Thus, for purposes of data analysis, they are classified as long-duration bursts. However, this necessitates a statistical correction to the resulting flux limits. We assume that up to 1/3 of these bursts may in fact be short-duration, based upon the standard ratio of short- to long-duration bursts observed by BATSE. So, of the 389 bursts known (or assumed) to be long-duration, 25 were excluded from the relevant limits, thus reducing the expected number of signal events by 25/389, or ~6%. This correction is likewise applied asymmetrically to the overall uncertainty.

B Green's Function Fluence Upper Limit Calculation

We show here sample calculations of the differential neutrino fluence upper limit, as well as a procedure to determine the integrated fluence and flux upper limits, following the Green's Function method set out in Section 3 of Fukuda et al. (2002). The fluence upper limit calculation assumes a monochromatic neutrino spectrum; the calculation is repeated at different values of the neutrino energy. The benefit of this method is that an integrated fluence upper limit can then be determined for any input spectrum, whether it be based on all of the bursts in this dataset or only on a subset of all bursts.

The fluence upper limit is defined as

$$F_\nu(E) \leq \frac{\mathrm{N}_{90}}{\mathrm{A}_{\mathrm{eff},\nu}(\mathrm{E}_\nu)} \tag{B.1}$$

where N_{90} is $\mu_{90}/\mathrm{N}_{\mathrm{Bursts}}$ and $\mathrm{A}_{\mathrm{eff},\nu}$ is the energy-dependent neutrino effective collecting area (see Section 3.3)[1].

Given $\mu_{90} = 1.30$ and $\mathrm{N}_{\mathrm{Bursts}} = 151$, then $\mathrm{N}_{90} = 8.61 \times 10^{-3}$. For $E_\nu = 100$ TeV (near the peak of the predicted neutrino flux), $A_{\mathrm{eff},\nu} = 5.0 \times 10^4$ cm^2, so F_ν(100 TeV) $\leq 1.7 \times 10^{-7}$ cm^{-2}. In Figure 4.2 we show F_ν as a function of energy as determined by the results of AMANDA's 2000-2003 observations. It is a straightforward matter to calculate these values for individual bursts or subsets of bursts. In addition to the flux prediction and the effective area as a function of energy, one needs only the background rate for the bursts in question ($R_{BG} \sim 4.5 \times 10^{-5}$ Hz on average, though this varies somewhat based upon the specific selection criteria applied) in order to determine the μ_{90} values and the F_ν values.

[1] Instead of using the neutrino effective area, one could also use the muon effective area multiplied by the neutrino to muon conversion probability (as in Fukuda et al. , 2002); in the case of AMANDA one must also account for attenuation of neutrinos in the earth.

We now determine the integrated fluence upper limit explicitly for an E^{-2} spectrum, as well the Waxman-Bahcall spectrum. First, the integrated fluence, F_{int} for an E^{-2} spectrum is

$$F_{\rm int} \leq [\int_{250\rm GeV}^{10^7\rm GeV} \frac{CE_\nu^{-2}}{F(E)} {\rm dE}_\nu]^{-1} = 1.4\times10^{-5}{\rm cm}^{-2}, \tag{B.2}$$

where C is the factor required to normalize the neutrino spectrum to unity—in this case, C = 250 GeV. This integrated fluence upper limit is significantly lower than the results of similar calculations performed by Fukuda et al. (2002) (we combine the ν_μ and $\bar{\nu}_\mu$ fluences into a single limit, while they present two separate fluence upper limits). However, a direct, quantitative comparison between these two results cannot be made due to the vastly different energy ranges of the two instruments. Note also the limits of integration employed here—though AMANDA is sensitive to neutrinos at higher and lower energies, the vast majority of the flux from GRBs is expected to come from neutrinos of a few hundred GeV to a few PeV.

Now we determine the integrated fluence upper limit for the Waxman-Bahcall spectrum, to provide a further example of the wide applicability of the Green's Function method:

$$F_{\rm int} \leq [\int_{250\rm GeV}^{10^5\rm GeV} \frac{CE_\nu^{-1}E_{\rm Break}^{-1}}{F(E)} {\rm dE}_\nu + \int_{10^5}^{10^7} \frac{CE_\nu^{-2}}{F(E)} {\rm dE}_\nu]^{-1} = 5.3\times10^{-7}{\rm cm}^{-2}, \tag{B.3}$$

where C again is the constant required to normalize the overall spectrum to unity; here $C = 7.0\times10^{-5}$GeV.

Finally, we compare this fluence upper limit to the flux upper limit derived for the Waxman-Bahcall spectrum in Section 4. To do this, we must convert the integrated fluence upper limit into a differential all-sky flux upper limit per burst; that is, from units of cm^{-2} to units of $GeV^{-1}cm^{-2}s^{-1}sr^{-1}$:

$$\frac{F_{\rm int}}{\Omega {\rm t}} = \frac{5.3{\times}10^{-7}}{(4\pi)(3.15{\times}10^{7}/700)} = 9.4 \times 10^{-13}{\rm cm}^{-2}{\rm s}^{-1}{\rm sr}^{-1}. \tag{B.4}$$

Next, we multiply by the normalization of the energy spectrum and take the differential to provide a flux upper limit of
$E^2\Phi_\nu \leq 1.3 \times 10^{-8}$ GeVcm^{-2}s^{-1}sr^{-1}.
This is nearly identical to the flux upper limit derived in the manner described in Section 3 for 151 bursts from 2000 to 2003 (see also Chapter 4, where we show that an MRF of 2.5 yields a flux upper limit of $E^2\Phi_\nu \leq 1.1 \times 10^{-8}$ GeVcm^{-2}s^{-1}sr^{-1}, consistent with the result derived in this section, to within the applicable uncertainties).

Thus we show that the Green's Function Method agrees with calculations which explicitly incorporated prior assumptions about the GRB neutrino spectrum. Therefore, this alternate method provides a powerful tool for determining the flux upper limit based on AMANDA observations for any proposed neutrino spectrum.

C Expanding the GRB Search to Other Transient Point Sources

While this work has provided the most stringent upper limit to date specifically for muon neutrino flux for gamma-ray bursts in coincidence with photon observations, the method described above can be expanded to search for other transient point sources as well. X-ray flares occurring minutes to hours after a GRB are thought to be caused by re-activation of the GRB central engine, and are a natural candidate for correlated neutrino searches (Murase & Nagataki , 2006b). Additionally, photon emission from supernovae could be used as a key element in searches for neutrino emission from jet-driven supernovae and γ-ray dark ("choked") GRBs (Razzaque et al. , 2003b). Jet-driven supernovae are expected to accelerate baryonic material to mildly relativistic energies (the Lorentz boost $\Gamma \sim$ a few), which may subsequently result in significant neutrino emission (Ando & Beacom , 2005). Not all supernovae will be jet-driven, but population estimates vary between 0.2% and 25% of all type Ib/c SNe (van Putten , 2004; Berger et al. , 2003; Soderberg , 2005). Given the number of such supernovae observed annually, it is reasonable to search for a neutrino signal from these events.

Another reason to search for neutrino emission from supernovae becomes apparent when we consider the recently-established SN-GRB connection. Several supernovae (including 1998bw and 2003dh) are known to be associated with GRBs. Furthermore, Razzaque et al. (2003b) describe a scenario where as many as 10^3 times the standard number of GRBs occur, though in these bursts the photon jet does not succeed in escaping the stellar envelope (the γ-ray dark GRBs). For these types of bursts, no gamma-rays will be observed. However, if even a fraction of these GRBs are associated with SNe (the fraction for observed GRBs has been calculated to be in the range of 10^{-2} to 10^{-3} (Bissaldi et al. , 2006)), then it will be possible to search for neutrinos in the time period surrounding the SN emission (provided the SN start time, the GRB time delay relative to the SN, and the duration of the GRB can be estimated with sufficient precision). Because these SNe are localized transient phenomena, the primary selection criteria for the GRB analysis (spatial and temporal correlation) are an excellent starting point for such a search, though it is possible that not all of the other data quality cuts used in the GRB search would be optimal for a supernova search. Finally, it is also possible to complement any of the transient point source searches described above by inverting the search algorithm, that is, by implementing Target of Opportunity photon searches based on spatio-temporal localization of potential neutrino events (Kowalski & Mohr , 2007). Any of these searches can potentially be of great benefit to the long-term goals of multi-messenger astronomy.

Bibliography

Achterberg, A. et al., ApJ, in press (astro-ph/0702265)

Achterberg, A. et al., submitted to PRD, November 2006 (astro-ph/0611063)

Achterberg, A. et al., Astropart. Phys. **26** (2006) 155 (astro-ph/0604450)

Ackermann, M. et al., J. Geophys. Res. **111** (2006), D13203

Aguilar, A.J. et al., Astropart. Phys. **26** (2006) 314-324; see also the Antares Neutrino Telescope Page: http://antares.in2p3.fr

Aharmim, B. et al., NIM **A449** (2000) 172-207

Ahrens, J. et al., NIM **A54** (2004) 169

Ahrens, J. et al., PRL **90** (2003) 251101

Ahrens, J. et al., ApJ **583** (2003) 1040

Ahrens, J. et al., PRD **66** (2002) 012005

Andrés, E. et al., Nature **410** (2001) 441-443

Ando, S. and J. Beacom, PRL **95** (2005) 061103

Bay, R.C. Ph.D. Thesis, University of California (2000) (astro-ph/0008255)

Berger, E. et al., ApJ **599** (2003) 408

Bissaldi, E. et al., A&A, in press (astro-ph/0702652)

Burrows, D. et al., Space Sci. Rev. **120** (2005) 165; see also the Swift Gamma-Ray Burst Mission Page: http://swift.gsfc.nasa.gov/docs/swift/swiftsc.html

Carson, J. for the GLAST Collaboration, Proc. 2nd TeV Workshop, Madison, WI (2006) (astro-ph/0610960); see also the GLAST Mission Page: http://glast.gsfc.nasa.gov

Chirkin, D. and W. Rhode, hep-ph/0407075

Conrad, J. et al., PRD **67** (2003) 012002

Costa, E. et al., Nature **386** (1997) 686-688

Dado, S. et al., astro-ph/0406325

Dar, A., Chin. J. Astron. Astrophys. **6** (2006) 301 (astro-ph/0511622)

Dar, A. et al., astro-ph/0611369

Dar, A. and A. DeRújula, astro-ph/0105094

DePaolis, F. et al., Astropart. Phys. **18** (2002) 249-260 (astro-ph/0107589)

Dermer, C. and A. Atoyan, New Journal of Physics **8** (2006) 122 (astro-ph/0606629)

Dermer, C. and A. Atoyan, PRL **91** (2003) 1102

Dermer, C. and A. Atoyan, New Astron. Rev. **48** (2004) 453-458 (astro-ph/0312591)

Eicher, D. et al., Nature **340** (1989) 126-128

Feldman, G. and R. Cousins, PRD **57** (1998) 3873-3889

Fishman, G.J. et al., A&A Supp **97** (1993) 17-20

Frail, D. et al., ApJ **562 L**55-58 (2001)

Franckowiak, A., Diploma Thesis in Preparation (2007)

Fryer, C. and P. Mészáros, ApJ **588 L**25-28 (2003)

Fukuda, S. et al., ApJ **578** (2002) 317

Gandhi, R. et al., PRD **58** (1998) 093009

Gandhi, R. et al., Astropart. Phys. **5** (1996) 81-110

Gupta, N., PRD **65** (2002) 113005 (astro-ph/0201509)

Hardtke, R., Ph.D. Thesis, University of Wisconsin (2002)

Heck, D. et al., Report FZKA 6019 (1998). An update of the original Corsika (6.030) was used in this analysis. See http://www-ik.fzk.de/corsika/ for additional information and more recent versions.

Hill, G.C. and K. Rawlins, Astropart. Phys. **19** (2003) 393

Hill, G.C., Astropart. Phys. **6** (1997) 215

Hillas, A.M., astro-ph/0607109

Hodges, J. for the IceCube Collaboration, Proc. 2nd TeV Workshop, Madison, WI (2006) (astro-ph/0611597)

Hodges, J., Ph.D. Thesis, University of Wisconsin (2007)

Hurley, K. et al., in "Compact Stellar X-Ray Sources", Lewin, W. et al., Eds. Cambridge University Press, Cambridge (2006)

Lyutikov, M., and R. Blandford, astro-ph/0312347

Hurley, K., Astron. Telegram #19 (1998)

Kalmykov, N. and S. Ostapchenko, Phys. Atom. Nucl. **56** (1993) 346

Kashti, T. and E. Waxman, PRL **95** (2005) 181101

Kommers, J. Ph.D. Thesis, MIT (1998); see also http://space.mit.edu/BATSE

Kowalski, M. and A. Mohr, astro-ph/0701618

Kuehn, K., http://icecube.wisc.edu/~kuehn/grb9703.html (AMANDA-GRB Supplemental Information Page)

Lipari, P. and T. Stanev, PRD **44** (1991) 113543

Markwardt, C.B. et al., ApJ **633 L**77-80 (2005)

Murase, K. and S. Nagataki, PRD **73** (2006) 063002

Murase, K. and S. Nagataki, PRL **97** (2006) 051101 (astro-ph/0604437)

Murase, K. and S. Nagataki, private communication (2006)

Paczyński, B., ApJ **494 L**45 (1998)

Piran, T., Rev. Mod. Phys. **76** (2004) 1143

Piran, T., Science **295** (2002) 986

Razzaque, S. et al., PRD **68** (2003) 3001

Razzaque, S. et al., PRL **90** (2003) 241103

Resvanis, L.K. et al., Nuc. Phys. B Proc. Supp. **122** (2003) 24-39; see also the NESTOR Institute for Astroparticle Physics Page: http://www.nestor.org.gr

Roming, P.W.A. et al., ApJ **651** (2006) 985 (astro-ph/0605005)

Soderberg, A. Nuovo Cim. 28C (2005) 563-573

Spiering, C. et al., astro-ph/0404096

Stamatikos, M. for the IceCube Collaboration, et al. Proc. 29th ICRC, Pune, India (2005) 471-474 (astro-ph/0510336)

Stamatikos, M. for the IceCube Collaboration, and D. Band, AIP Conf. Proc. **836** (2006) 599 (astro-ph/0604281)

Stern, B.E. et al., ApJ **563** (2001) 80

Taylor, G. et al., ApJ **609 L**1-4 (2004) (astro-ph/0405300)

van Putten, M., ApJ **611 L**81-84 (2004)

Vietri, M., PRL **80** (1998) 3690(4)

Waxman, E., Nuc. Phys. B Proc. Supp. **118** (2003) 353-362 (and references therein)

Waxman, E. and J. Bahcall PRL **78** (1997) 2292